

Truncated Modular Exponentiation Operators: A Strategy for Quantum Factoring

Robert L. Singleton Jr.[†]
SavantX Research Center
Santa Fe, New Mexico, USA

(Dated: 6/5/2024)

Abstract

Modular exponentiation (ME) operators are one of the fundamental components of Shor's algorithm, and the place where most of the quantum resources are deployed. These operators are often referred to as the bottleneck of the algorithm. I propose a method for constructing the ME operators that requires only $3n + 1$ qubits with no ancillary qubits. The method relies upon the simple observation that the work register starts in state $|1\rangle$. Therefore, we do not have to create an ME operator U that accepts a *general* input, but rather, one that takes an input from the periodic sequence of states $|f(x)\rangle$ for $x \in \{0, 1, \dots, r - 1\}$. Here, the ME function with base a is defined by $f(x) = a^x \pmod{N}$ and has a period of r . For an n -bit number N , the operator U can be partitioned into r levels, where the gates in level $x \in \{0, 1, \dots, r - 1\}$ increment the state $|f(x)\rangle = |w_{n-1} \dots w_1 w_0\rangle$ to the state $|f(x+1)\rangle = |w'_{n-1} \dots w'_1 w'_0\rangle$. The gates below x do not affect the state $|f(x+1)\rangle$. This amounts to transforming an n -bit binary number $w_{n-1} \dots w_1 w_0$ into another binary number $w'_{n-1} \dots w'_1 w'_0$, without altering the previous states, which can be accomplished by a set of formal rules involving multi-control-NOT gates and single-qubit NOT gates. The process of gate construction can therefore be automated, which is essential for factoring larger numbers. The obvious problem with this method is that it is self-defeating: If we knew the operator U , then we would know the period r of the ME function, and there would be no need for Shor's algorithm. I show, however, that the ME operators are very forgiving, and truncated approximate forms in which levels have been omitted are able to extract factors just as well as the exact operators. I demonstrate this by factoring the numbers $N = 21, 33, 35, 143, 247$ by using less than half the requisite number of levels in the ME operators. This procedure works because the method of continued fractions only requires an approximate phase value, which suggests that implementing Shor's algorithm might not be as difficult as first suspected. This is the basis for a factorization strategy in which one level at a time is iterated over using an automated script. In this way, we fill the circuits for the ME operators with more and more gates, and the correlations between the various composite operators U^p (where p is a power of two) compensate for the missing levels.

[†] corresponding email: robert.singleton@savantx.com or bobs1@comcast.net

CONTENTS

I. Introduction	3
II. Review of Shor's Algorithm	6
III. Truncated Modular Exponentiation Operators	13
A. $N = 21 = 3 \times 7$, $a = 2$, $r = 6$	15
B. $N = 33 = 3 \times 11$, $a = 7$, $r = 6$	23
C. $N = 143 = 11 \times 13$, $a = 5$, $r = 20$	27
D. $N = 247 = 13 \times 19$, $a = 2$, $r = 36$	32
IV. Conclusions	37
Acknowledgments	39
A. Modular Exponentiation Operators	39
1. Modular Exponentiation Operators for $N = 143$	39
2. Modular Exponentiation Operators for $N = 247$	41
References	44

I. INTRODUCTION

Modern computer security relies upon RSA encryption and related methods [1–3]. Very large semi-primes N are used to create *public-private* key pairs based upon the factors of N . The number N is called the *public key*, and it can be known to everyone. It is typically thousands of bits long; for example, standard RSA can employ keys of 4096-bits and larger. The *private key*, *i.e.* the factors of N , must remain secret. Indeed, if we knew the private key, this would break the encryption. Therefore, the security of these schemes rests upon the fact (or rather the empirical observation) that it is very hard to factor large numbers. A classical digital computer must essentially check every combination of factors in succession, and breaking a 4096-bit key would take much longer than the age of the universe, even on the largest high performance supercomputers. In contrast, Shor’s algorithm [4, 5] runs on a quantum computer, exploiting the massive parallelism inherent in quantum mechanics, so that all numbers can be tested simultaneously rather than sequentially. This provides for a *polynomial* factorization method. Thus, by employing quantum processes, Shor’s algorithm can factor large numbers exponentially faster than a classical computer, placing the security of RSA in grave danger.¹

Just how close are we to manufacturing an existing quantum device that can perform multipurpose factoring of large numbers relevant for encryption? To address this question, it is necessary to assess the current experimental state of quantum factoring. The first factorization was performed in 2001 in Ref. [6], which factored $N = 15$ using an NMR device with 7 qubits. Over the following decade, a number of experiments were fielded that employed photonic devices, which factored $N = 15$ and $N = 21$ [7–10]. Significantly, these experiments observed entanglement, which is essential for a quantum speedup. Finally, over the last decade, the numbers $N = 15, 21, 35$ were factored using a trapped ion device and IBM’s superconducting qubits [11–13], although $N = 35$ had a success rate of only 14%. All of these experiments have relied upon some form of simplification to reduce the qubit and gate count, but they successfully provide proof-of-principle demonstrations of the feasibility of Shor’s algorithm.

These are indeed seminal experiments, and they have pushed the limits of existing technology. However, in some sense, only modest progress has been made over the last 20 years, and it is clear that decoherence remains the primary obstacle. It is encouraging, however, that the rate of progress seems to be increasing. The experiments have all been confined to small numbers, $N = 15, 21, 35$, and small periods such as $r = 2, 3, 4$. All but Ref. [6] employs some type of *compiled* algorithm, in which knowledge of the solution is exploited

¹ It is indeed ironic to think that the digital security of entire nations and the world economy rests upon the *assumption* that factoring is difficult.

to decrease the number of qubits and gates on the machine. All current machines lack a sufficient number of qubits and acceptable decoherence times to run a full non-compiled version of Shor’s algorithm, even for small numbers. The qubit count for a full version of Shor is just too demanding. For example, for an $n = 4096$ bit number N , the method proposed in this manuscript would require $3n + 1 = 12289$ total qubits. The gate count for the modular exponential (ME) operator is also problematic. To this point, the general purpose ME operator of Ref. [14] requires of order $72n^3$ gates for an n -bit number. Therefore, the ME operator for a 4096-bit key would need 5×10^{12} gates! Breaking RSA consequently requires tens of thousands or even trillions of high quality gates, in addition to very long decoherence times. Modern quantum computers are currently quite far from this domain, although future machines will undoubtedly be able to handle these requirements. Quantum computers must first emerge from the Noisy Intermediate-Scale Quantum (NISQ) regime [15] before large numbers can be factored using a full implementation of Shor’s algorithm (rather than compiled versions with semi-classical Fourier transforms). But there is every reason to believe that at some point in the not too distant future, quantum computers will be able to break RSA keys of length 4096 and higher.

The ME operators are the most critical component of Shor’s algorithm. These operators are also responsible for the entanglement of the quantum system, which is required for a quantum speedup. Shor’s algorithm is based on the observation that factoring a semi-prime number N is equivalent to finding the period r of the ME function $f(x) = a^x \pmod{N}$. The number a is called the *base*, and it is chosen randomly such that $1 < a < N$ and $\gcd(a, N) = 1$. The number of bits required to represent a number N is given by $n = \lceil \log_2 N \rceil$, and the ME operator U acts on an n -bit *work register* to transform the state $|f(x)\rangle$ to the next state $|f(x+1)\rangle$ for $x \in \{0, 1, 2, \dots\}$. This procedure lies at the heart of Shor’s algorithm, and consumes the most quantum resources. One can fairly say that implementing the ME operator is the primary bottleneck of the algorithm. The method introduced in Ref. [16] (and presented in this manuscript) is designed to reduce the gate count dramatically, and relies on the following observation. Since the work register starts in state $|1\rangle$, we do not have to create an ME operator U that takes a *general* input, as in Ref. [14]. Rather, we can use only the inputs from the periodic sequence of states $|f(x)\rangle$ for $x \in \{0, 1, \dots, r-1\}$. An ME operator U with period r can therefore be partitioned into r segments indexed by the integers $x \in \{0, 1, \dots, r-1\}$. The gates in segment x transform the work-state $|f(x)\rangle \equiv |w_{n-1} \dots w_0\rangle$ into $|f(x+1)\rangle \equiv |w'_{n-1} \dots w'_0\rangle$, while the levels below x have no effect on the state $|f(x+1)\rangle$. Transforming a binary state $w_{n-1} \dots w_0$ into another binary state $w'_{n-1} \dots w'_0$, without altering the preceding states, can be turned into a set of formal rules involving multi-control-NOT gates and single-qubit NOT gates. This procedure can therefore be automated, which will be

essential for factoring large numbers. Indeed, this is how most of the gates in this manuscript and in Ref. [16] were constructed.

There is an obvious problem with this method, however. Knowing the operator U is equivalent to knowing the period of the modular exponentiation function $f(x)$, which means that Shor's algorithm is not needed. However, it turns out that the entire sequence of transitions that define the U operator is *not* required. We can instead use *truncated* approximate versions of the ME operators in which levels are omitted. The corresponding phase histograms show that employing this truncation strategy still permits us to extract the appropriate phases, and therefore the correct factors. This is because the method of continued fractions uses only an *approximate* phase in order to extract the period of $f(x)$, and omitting levels in U still provides an adequate approximation for the measured phase that determines the period. I will perform a number of systematic truncation studies, with the general result that well over half the requisite number of levels can be omitted without affecting the ability to factor. This makes factorization much easier, and provides for a practical factorization strategy in which the ME operators are constructed one level at a time from the bottom up.

This paper is organized as follows. To establish notation and context, Section II presents a brief review of Shor's algorithm. The theory of ME operators and the proposed method for constructing them are introduced in Section III. I use this truncated formalism to factor the numbers $N = 21, 33, 35, 143, 247$, carrying out corresponding systematic truncation studies. It should be emphasized that factorization can still be performed when well over half of the levels of the ME operators are omitted. Finally, Section IV provides some concluding remarks and potential paths for future research.

II. REVIEW OF SHOR'S ALGORITHM

I shall now present a review of Shor's algorithm. To establish some notation, we first look at the qubit ordering convention employed by OpenQASM/Qiskit [17]. For an m -qubit system, the computational basis states start with qubit 0 in the upper position, working their way down to the last qubit labeled by $m - 1$ (in both the quantum circuit and the tensor product representation). The basis states can therefore be expressed by

$$|k\rangle = |k_0\rangle \otimes |k_1\rangle \otimes \cdots \otimes |k_{m-2}\rangle \otimes |k_{m-1}\rangle, \quad (2.1)$$

where $k_\ell \in \{0, 1\}$. There are $M = 2^m$ quantum states in the system, with each state being indexed by an m -bit integer $k \in \{0, 1, \dots, M - 1\}$. In binary form, these integers are represented by

$$k = k_{m-1}k_{m-2} \cdots k_1k_0 \quad (2.2)$$

$$= 2^{m-1}k_{m-1} + 2^{m-2}k_{m-2} + \cdots + 2^1k_1 + 2^0k_0, \quad (2.3)$$

where k_0 is the least significant bit. The OpenQASM/Qiskit bit-convention is shown in Fig. 1, and we will use this convention throughout the manuscript. This convention is more in line with computer science, and differs slightly from the convention employed in physics. Note that the relation

$$\theta_k \equiv \frac{k}{M} = \frac{k_{m-1}}{2^1} + \frac{k_{m-2}}{2^2} + \cdots + \frac{k_1}{2^{m-1}} + \frac{k_0}{2^m} \quad (2.4)$$

$$= 0.k_{m-1} \cdots k_1k_0 \quad (2.5)$$

is an m -bit phase angle between 0 and 1. Given any m -bit phase θ_k , we will often use the fact that $M\theta_k = k$ is an m -bit integer between 0 and $M - 1$.

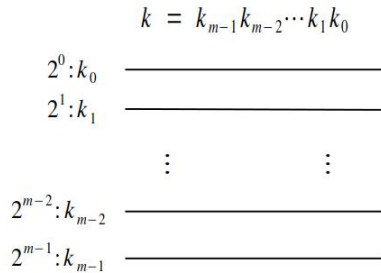


FIG. 1. An m -bit binary integer k can be encoded on a gated quantum computer using a number of bit-conventions. The OpenQASM/Qiskit convention starts at the top with qubit 0, and works its way down to the last qubit labeled by $m - 1$. Binary integers are expressed by the standard bit encoding $k = k_{m-1} \cdots k_1k_0$, which places the lowest order bit k_0 at the top of the circuit.

Now that the qubit ordering conventions have been defined, I am ready to summarize Shor's algorithm, which rests upon two fundamental quantum algorithms: the quantum Fourier transform (QFT), and the quantum phase estimation (QPE). The QFT implements the discrete Fourier transform on a gated quantum computer, and like the classical Fourier transform, it extracts frequency signals from an input source. The QPE algorithm, in contrast, finds the complex phases or the eigenvalues of an arbitrary *unitary* linear operator. Shor's algorithm elegantly combines the QFT and QPE to construct a powerful quantum algorithm for factoring very large integers. The mathematics behind Shor's algorithm is based on a simple but profound result from number theory, which maps the factoring problem onto another mathematical problem that finds the period of the *modular exponential function*. The period of this function is directly related to the factors of the number in question, and the QPE extracts this period using the method of continued fractions, thereby providing the sought after factors.

The general circuit for Shor's algorithm is illustrated in Fig. 2. Two registers are required: (i) a control register of m qubits, and (ii) a work register of n qubits. The work register stores all possible values of the modular exponentiation (ME) function

$$f(x) = a^x \pmod{N}, \quad (2.6)$$

where a is called the *base*, and it satisfies the conditions $1 < a < N$ and $\gcd(a, N) = 1$. The factors of N are related to the period r of the ME function by $\gcd(a^{r/2} \pm 1, N)$. Since

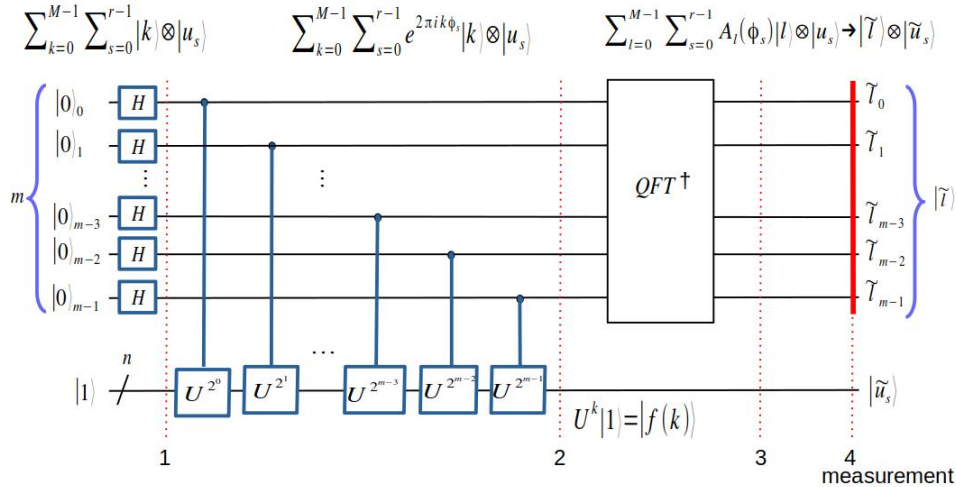


FIG. 2. Shor's algorithm for factoring a semi-prime N in the OpenQASM/Qiskit convention. There are two registers, a control register containing m qubits, and a work register containing n qubits, with $n = \lceil \log_2 N \rceil$. Measuring the control register projects the system into a state $|\tilde{\ell}\rangle \otimes |\tilde{u}_s\rangle$ for some index $\tilde{\ell} = \tilde{\ell}_{m-1} \dots \tilde{\ell}_0 \in \{0, 1, \dots, M-1\}$ and some ME eigenstate $|\tilde{u}_s\rangle$, where $M = 2^m$ is the number of quantum states in the control register. This gives the m -bit measured phase $\tilde{\phi} = \tilde{\ell}/M = 0.\tilde{\ell}_{m-1} \dots \tilde{\ell}_1 \tilde{\ell}_0$, which lies close to the actual phase ϕ_s with high probability. Upon knowing $\tilde{\phi}$, we can extract the exact phase $\phi_s = s/r$ using the method of continued fractions.

the values of $f(x)$ lie between 0 and $N - 1$, we choose the number of work qubits to be $n = \lceil \log_2 N \rceil$. The control register, which might also be called the period register or the *phase register*, stores all possible m -bit approximations to the eigenphases of the corresponding ME operator. Note that there are $M = 2^m$ quantum states in the control register. The continued fractions algorithm dictates that the number of qubits should be set to $m = 2n + 1$ for sufficient phase resolution [18]. The work-space states are indexed by an n -bit binary integer $w = w_{n-1} \cdots w_1 w_0$, where $w \in \{0, 1, \dots, 2^n - 1\}$. We will denote states in the work register by either their binary representation $|w_{n-1} \cdots w_1 w_0\rangle_w$, or by their numerical form $|w\rangle_w$ (usually the later). These states can be viewed as the computational basis for the work register, and therefore linear operators are specified by their action on these states.

The modular exponentiation (ME) operator for Shor's algorithm is defined by

$$U_{a,N} |w\rangle_w = |a \times w \pmod{N}\rangle_w, \quad (2.7)$$

and therefore

$$U_{a,N} |f(x)\rangle_w = |f(x+1)\rangle_w, \quad \text{or equivalently} \quad (2.8)$$

$$U_{a,N}^x |1\rangle_w = |f(x)\rangle_w \quad \text{for any } x \in \{0, 1, 2, \dots\}. \quad (2.9)$$

We will use the short-hand notation $U = U_{a,N}$ in the future, with the base a and the number N being left implicit. The eigenvalue problem for the ME operator U can be expressed by

$$U|u_s\rangle_w = e^{2\pi i \phi_s} |u_s\rangle_w \quad \text{where } \phi_s = \frac{s}{r} \quad \text{with } s \in \{0, 1, \dots, r-1\}, \quad (2.10)$$

and the eigenstates are given by

$$|u_s\rangle_w = \frac{1}{\sqrt{r}} \sum_{k=0}^{r-1} e^{-2\pi i k \phi_s} |f(k)\rangle_w. \quad (2.11)$$

By using the relation

$$\sum_{s=0}^{r-1} e^{2\pi i k \phi_s} = r \delta_{k,0} \quad (2.12)$$

for any integer k , we can invert (2.11) to obtain

$$|f(k)\rangle_w = \frac{1}{\sqrt{r}} \sum_{s=0}^{r-1} e^{2\pi i k \phi_s} |u_s\rangle_w. \quad (2.13)$$

It is clear from (2.13) that $|f(k)\rangle_w$ is periodic in k with period r . Note that for $k = 0$, we find the interesting expression

$$|1\rangle_w = |0 \cdots 01\rangle_w = \frac{1}{\sqrt{r}} \sum_{s=0}^{r-1} |u_s\rangle_w. \quad (2.14)$$

Thus, populating the work register with state $|1\rangle_w$ is equivalent to filling that register with a uniform linear sum of the eigenstates $|u_s\rangle_w$ for all values of s . This is the origin of the entanglement between the work and control registers. We are now ready to commence with Shor's algorithm.

- (i) To factor a semi-prime number N , randomly choose a base a such that $1 < a < N$ and $\gcd(a, N) = 1$ (if there *were* non-trivial common factors of a and N , then we have found a factor of N , which was the objective). The ME function $f(x)$ is now defined as in (2.6), and we seek the period r of this function, that is to say, the smallest positive integer r such that $a^r \pmod{N} = 1$. If $\gcd(a, N) = 1$, such a period $r \leq N$ always exists.
- (ii) The control and work registers are initialized to the state

$$|\psi_0\rangle = |\underbrace{00\cdots 0}_m\rangle_c \otimes |\underbrace{0\cdots 01}_n\rangle_w = |0\rangle_c \otimes |1\rangle_w . \quad (2.15)$$

- (iii) Hadamard gates $H^{\otimes m}$ act on the control register to create the uniform distribution

$$|\psi_1\rangle = \frac{1}{\sqrt{M}} \sum_{k=0}^{M-1} |k\rangle_c \otimes |1\rangle_w \quad (2.16)$$

$$= \frac{1}{\sqrt{rM}} \sum_{k=0}^{M-1} \sum_{s=0}^{r-1} |k\rangle_c \otimes |u_s\rangle_w , \quad (2.17)$$

where the number of quantum states in the control register is $M = 2^m$. I have used (2.14) in passing from the first form of state-1 to the second form, which is more convenient when taking the inverse QFT later in the circuit. The Hadamard gates ensure that all possible combinations of k can be processed simultaneously via the massive parallelism of quantum mechanics.

- (iv) Controlled modular exponentiation operators CUP for $p \in \{2^0, 2^1, \dots, 2^{m-1}\}$ act between the control and work registers to form the highly entangled state

$$|\psi_2\rangle = \frac{1}{\sqrt{rM}} \sum_{k=0}^{M-1} \sum_{s=0}^{r-1} e^{2\pi i k \phi_s} |k\rangle_c \otimes |u_s\rangle_w \quad (2.18)$$

$$= \frac{1}{\sqrt{M}} \sum_{k=0}^{M-1} |k\rangle_c \otimes |f(k)\rangle_w , \quad (2.19)$$

where I have used (2.13) in passing from the first form to the second form of state-2. These two equivalent forms express different ways of thinking about the state after the controlled ME operators CUP have acted. Figure 2 emphasizes forms (2.18) and (2.17) expressed in terms of the eigenphases $|u_s\rangle$. See Fig. 3 and the surrounding discussion for an explanation of the role of phase kickback and entanglement in expression (2.18).

- (v) The previous state involves the Fourier transform of the phases ϕ_s . These phases can therefore be recovered with an inverse Fourier transform applied to the control register, which takes the form

$$QFT_c^\dagger = \frac{1}{\sqrt{M}} \sum_{\ell=0}^{M-1} \sum_{k=0}^{M-1} e^{-2\pi i k \ell / M} |\ell\rangle \langle k|_c . \quad (2.20)$$

The final state therefore becomes

$$|\psi_3\rangle = QFT_c^\dagger |\psi_2\rangle = \sum_{\ell=0}^{M-1} \sum_{s=0}^{r-1} A_\ell(\phi_s) |\ell\rangle_c \otimes |u_s\rangle_w , \quad (2.21)$$

where the amplitudes are given by

$$A_\ell(\phi_s) = \frac{1}{\sqrt{r}M} \sum_{k=0}^{M-1} e^{2\pi i k (\phi_s - \ell/M)} \quad (2.22)$$

$$= \frac{1}{\sqrt{r}M} \frac{1 - e^{2\pi i (\phi_s - \ell/M)M}}{1 - e^{2\pi i (\phi_s - \ell/M)}} . \quad (2.23)$$

- (vi) We now measure the control register to obtain $\tilde{\ell} = \tilde{\ell}_{m-1} \cdots \tilde{\ell}_1 \tilde{\ell}_0$. Dominant peaks occur at the phase values $\tilde{\phi} = \tilde{\ell}/M = 0.\tilde{\ell}_{m-1} \cdots \tilde{\ell}_1 \tilde{\ell}_0$ near the exact ME phases $\phi_s = s/r$ for $s \in \{0, 1, \dots, r-1\}$. The continued fractions algorithm is then applied to the control register to extract the integers s and r of the exact phase $\phi_s = s/r$. As a practical matter, for the continued fractions algorithm to work, the integers s and r can have no non-trivial common factors. This slightly reduces the number of reliable peaks from which r can be obtained. The number of control qubits is required to be $m = 2n + 1$, so that $\tilde{\phi}$ has enough resolution to reliably extract the phase $\phi_s = s/r$ using the continued fractions method [18]. If the period turns out to be odd, then return to step (i) and choose another base a (unless a is a perfect square). Otherwise, check that $a^{r/2} \not\equiv -1 \pmod{N}$ and that $a^r \equiv 1 \pmod{N}$. Note that $a^{r/2} \not\equiv 1 \pmod{N}$ holds automatically (otherwise the period would be $r/2$ rather than r). If these conditions are not met, then return to (ii) and try again. The probability of success is quite high after only a few iterations. Once a solution for r is obtained, proceed to the next and final step.

- (vii) The factors are given by $\gcd(a^{r/2} \pm 1, N)$. The greatest common divisor can be calculated quickly using Euler's algorithm on a classical computer.

The modular exponentiation operator of (iv) is the most crucial component of Shor's algorithm, and it is useful to review it further, with an eye on entanglement. Let us start with a single eigenstate $|u_s\rangle$ in the work register. The control and work subscripts have been dropped for readability. A series of controlled operators CU^p with control qubit $q \in \{0, 1, \dots, m-1\}$

and power $p \in \{2^0, 2^1, \dots, 2^{m-1}\}$ act on the work register. Each power p corresponds to a power of 2 in the binary representation of an m -bit number $k = k_{m-1} \dots k_1 k_0$ in the control register. After the action of the controlled ME operator CU^p (position-2 in Fig. 2), phase kickback produces the state

$$CU^p H|0\rangle \otimes |u_s\rangle = \frac{1}{\sqrt{2}} |0\rangle \otimes |u_s\rangle + \frac{1}{\sqrt{2}} |1\rangle \otimes U^p |u_s\rangle \quad (2.24)$$

$$= \frac{1}{\sqrt{2}} |0\rangle \otimes |u_s\rangle + \frac{1}{\sqrt{2}} |1\rangle \otimes e^{2\pi i p \phi_s} |u_s\rangle \quad (2.25)$$

$$= \frac{1}{\sqrt{2}} \left(|0\rangle + e^{2\pi i p \phi_s} |1\rangle \right) \otimes |u_s\rangle. \quad (2.26)$$

This procedure is represented in Fig. 3 for the state $|u_s\rangle$ in the work register. The system is now in the state

$$|\psi_2^s\rangle = \frac{1}{2^{m/2}} \left(|0\rangle + e^{2\pi i 2^0 \phi_s} |1\rangle \right)_0 \otimes \dots \otimes \left(|0\rangle + e^{2\pi i 2^{m-1} \phi_s} |1\rangle \right)_{m-1} \otimes |u_s\rangle \quad (2.27)$$

$$= \frac{1}{2^{m/2}} \sum_{k_0=0,1} e^{2\pi i 2^0 \cdot k_0} |k_0\rangle \otimes \dots \otimes \sum_{k_{m-1}=0,1} e^{2\pi i 2^{m-1} \cdot k_{m-1}} |k_{m-1}\rangle \otimes |u_s\rangle \quad (2.28)$$

$$= \frac{1}{2^{m/2}} \sum_{k_0=0,1} \dots \sum_{k_{m-1}=0,1} e^{2\pi i \phi_s (2^0 k_0 + \dots + 2^{m-1} k_{m-1})} |k_0\rangle \otimes \dots \otimes |k_{m-1}\rangle \otimes |u_s\rangle \quad (2.29)$$

$$= \frac{1}{\sqrt{M}} \sum_{k=0}^{M-1} e^{2\pi i k \phi_s} |k\rangle \otimes |u_s\rangle \equiv |\text{control}\rangle \otimes |\text{work}\rangle. \quad (2.30)$$

Note that the control register for state (2.30) is entangled with itself (and indeed, this entanglement will produce the quantum speedup). However, the control and work registers

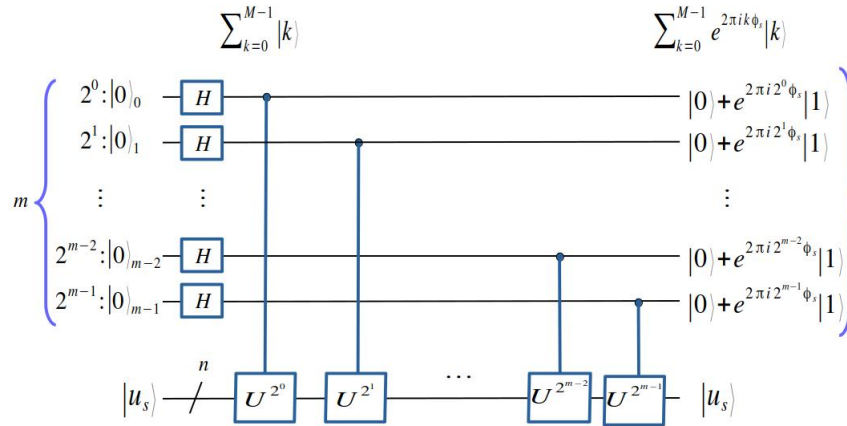


FIG. 3. Quantum phase estimation front-end in the OpenQASM/Qiskit convention. The work register has been populated by the eigenstate $|u_s\rangle$.

are not entangled, as $|\psi_2^s\rangle$ is a simple tensor product of a control state and a work state. However, if the work register is in state $|1\rangle$, then we must sum over all s with equal weights, so that

$$|\psi_2\rangle = \frac{1}{\sqrt{r}} \sum_{s=0}^{r-1} |\psi_2^s\rangle = \frac{1}{\sqrt{rM}} \sum_{k=0}^{M-1} \sum_{s=0}^{r-1} e^{2\pi i k \phi_s} |k\rangle \otimes |u_s\rangle, \quad (2.31)$$

from which state (2.18) is obtained. Thus, by starting the work register in state $|1\rangle$, entanglement between the control and work registers is introduced. This is why a measurement on the control register in Fig. 2 also projects the work register into an eigenstate of U . Although the work state is not measured, it might be interesting to do so for diagnostic purposes, but that is beyond the scope of this work.

It is informative to calculate $|\psi_2\rangle$ in yet another way. Suppose the control register is in the state $|k\rangle$, where $k = k_{m-1} \cdots k_1 k_0$, and take the work register to be in state $|1\rangle$. Then the action of the controlled ME operators CU^p produces the work-state

$$U^{2^0 \cdot k_0} \times U^{2^1 \cdot k_1} \times \cdots \times U^{2^{m-1} \cdot k_{m-1}} |1\rangle = U^k |1\rangle = |f(k)\rangle, \quad (2.32)$$

and state-2 becomes

$$|\psi_2\rangle = \frac{1}{\sqrt{M}} \sum_{k=0}^{M-1} |k\rangle \otimes |f(k)\rangle, \quad (2.33)$$

in agreement with (2.19). Upon employing (2.13), state-2 can be written in the first form (2.18). This is more convenient when taking the inverse QFT.

There is a further simplification when the ϕ_s are m -bit phases. In this case $\ell_s = M\phi_s$ is an integer between 0 and $M-1$, and $A_\ell(\phi_s) = \delta_{\ell, \ell_s} / \sqrt{r}$ [16]. Most amplitudes vanish, and there are only r non-zero values at $\ell = \ell_s$ for $s \in \{0, 1, \dots, r-1\}$, so that

$$|\psi_3\rangle = \frac{1}{\sqrt{r}} \sum_{s=0}^{r-1} |\ell_s\rangle \otimes |u_s\rangle. \quad (2.34)$$

There is a more revealing way of obtaining this result. Since $M\phi_s = \ell_s$ is an m -bit integer, note that (2.18) can be expressed in terms of an exact QFT,

$$|\psi_2\rangle = \frac{1}{\sqrt{r}} \frac{1}{\sqrt{M}} \sum_{k=0}^{M-1} \sum_{s=0}^{r-1} e^{2\pi i k \ell_s / M} |k\rangle \otimes |u_s\rangle = QFT \cdot \frac{1}{\sqrt{r}} \sum_{s=0}^{r-1} |\ell_s\rangle \otimes |u_s\rangle. \quad (2.35)$$

Upon taking the inverse QFT^\dagger , the final state is given by (2.34). This is the case for $N = 15$ where $r = 2, 4$ for all bases a . This does not occur, for example, with a period that contains the factor 3, since $1/3$ does not terminate. This explains the richer phase-structure for $N = 21$ (where $a = 2$ gives $r = 6$), and for larger numbers N .

III. TRUNCATED MODULAR EXPONENTIATION OPERATORS

Recall that the Shor factoring circuit of Fig. 2 possesses two registers: a control or phase register containing m qubits, and a work register containing $n = \lceil \log_2 N \rceil$ qubits, where N is the semi-prime number we wish to factor. For sufficient phase resolution in the continued fractions routine, the control register should contain $m = 2n + 1$ qubits, although in practice we can sometimes get by with fewer qubits. The modular exponentiation (ME) operators U^p for $p \in \{2^0, 2^1, \dots, 2^{m-1}\}$ act on the work register, and are the most crucial component of Shor's algorithm. They are often called the *bottleneck* of the algorithm. I would also refer to them as the *workhorse* of the procedure, as most of the quantum resources are deployed here. Furthermore, the ME operators are responsible for the entanglement of the control register, which is required for a quantum speedup. Shor's algorithm is based on the observation that the factors of a semi-prime number N are determined by the period r of the ME function $f(x) = a^x \pmod{N}$, and the algorithm is designed to extract this period. The ME function $f(x)$ is implemented by an ME operator U that performs the transitions $|f(x)\rangle \rightarrow |f(x+1)\rangle$ from one work-state to the next. As previously emphasized, the ME operators are indeed both the bottleneck and the workhorse of the procedure, as they require the largest expenditure of quantum resources. For example, constructing a general U operator can employ thousands of gates [14], each of which must maintain coherence with the others.

In Ref. [16], I recently proposed a method for reducing the gate count of the ME operators U^p with a total of $3n + 1$ qubits in the Shor circuit. This reference also serves as a thorough introduction to Shor's algorithm. I employed the Qiskit simulator to factor a variety of smaller numbers ($N = 15, 21, 33, 35$), as well as the larger semi-primes $N = 143, 247$. That smaller values of N could be factored in this way is not very remarkable, and serves to prove that the method is sound. But to my knowledge, numbers in the hundreds had never been factored before, and indeed pushed the limits of the simulator, even with the reduced gate count. Soon thereafter, Ref. [19] also factored $N = 143, 247$ on the Qiskit simulator using quite similar methods. However, the author used much smaller periods than Ref. [16]. For example, in factoring $N = 143$ and $N = 247$, Ref. [19] used the periods $r = 4$ ($a = 21$) and $r = 12$ ($a = 8$), respectively. This should be compared to Ref. [16], which factored these numbers using the much larger periods of $r = 20$ ($a = 5$) for $N = 143$ and $r = 36$ ($a = 2$) for $N = 247$. I used these larger periods in an effort to push the simulator and the continued fractions routine to their limits. Using such large periods was facilitated by the automation of the gate construction procedure, as making an ME operator with a period of $r = 36$ is just too time consuming and tedious to perform manually.

Reference [19] goes on to survey a large number of implementation strategies for ME operators. The author categorizes ME operators into three primary types: (i) those that employ basic arithmetic operations, (ii) those that employ Fourier rotations, and (iii) specially designed circuits. Examples of method (i) are given in Refs. [14] and [20]. Most notably, the general routine of Ref. [14] takes of order $72n^3$ gates for an n -bit ME operator. While the number of gates is *only* polynomial in n , the cubic growth renders the gate count far too large for current machines. Even the smallest number $N = 15$ for which Shor's algorithm is applicable would require 9000 gates with this procedure. An example of method (ii) is Ref. [21], which requires of order $2000n^2$ gates, and is therefore also out of current experimental reach. After a thorough review, Ref. [19] concludes that only method (iii) involving specially designed circuits is feasible for existing and near-term devices. The method of Ref. [16] falls into category (iii) of this taxonomy.

The proposed method is not really profound, and lies on the simple observation that

$$U|f(x)\rangle = |f(x+1)\rangle, \quad (3.1)$$

or equivalently,

$$U^x|1\rangle = |f(x)\rangle \text{ for any } x \in \{0, 1, 2, \dots\}, \quad (3.2)$$

where $f(x)$ is the ME function defined by (2.6). Since the work register starts in state $|1\rangle$, we do not have to create an ME operator U that takes a *general* input, but rather, one that takes an input from the periodic sequence of states $|f(x)\rangle$ for $x \in \{0, 1, 2, \dots\}$. An ME operator U with period r can therefore be partitioned into r segments indexed by the integers $x \in \{0, 1, \dots, r-1\}$. The gates in segment x transform the work-state $|f(x)\rangle \equiv |w_{n-1} \dots w_0\rangle$ into $U|f(x)\rangle = |f(x+1)\rangle \equiv |w'_{n-1} \dots w'_0\rangle$, while the levels below x have no effect on the state $|f(x+1)\rangle$. Transforming a binary number $w_{n-1} \dots w_1 w_0$ into another binary number $w'_{n-1} \dots w'_1 w'_0$, without altering the preceding states, can be turned into a set of formal rules involving multi-control-NOT gates $CC \dots CX$ and single-qubit NOT gates X . This procedure can therefore be automated. Indeed, this is how most of the gates in this manuscript and in Ref. [16] were constructed: The factorization script essentially wrote itself, including the Qiskit gate output for the next level of the ME operator U . The same script can be used for the composite operators U^p for $p \in \{2^0, 2^1, \dots, 2^{m-1}\}$. This method consequently requires $\mathcal{O}(m \times nr) \sim \mathcal{O}(n^2 r)$ gates, as each of the $m = 2n + 1$ operators U^p requires of order nr gates.

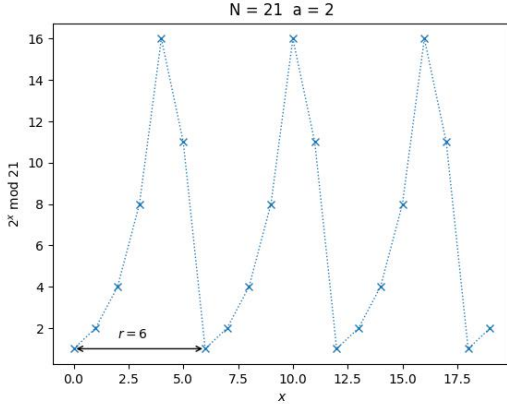
Let us make the following observation before continuing with an example. We shall denote the 2^n -dimensional space for the work-register by \mathcal{W}_n , and a general ME operator U can act on this entire Hilbert space. Consider now the r -dimensional subspace defined by

$$\mathcal{U}_r \equiv \text{Span} \left\{ |f(x)\rangle \mid x \in \{0, 1, \dots, r-1\} \right\} \subseteq \mathcal{W}_n. \quad (3.3)$$

As discussed above, the U operator transforms one basis element of \mathcal{U}_r into another basis element, that is to say, the ME operator U leaves the subspace \mathcal{U}_r invariant, so that $U[\mathcal{U}_r] = \mathcal{U}_r$. Thus, as the U operator acts successively, the states in the work register only vary over the r -dimensional subspace \mathcal{U}_r . This means that the subspace \mathcal{U}_r is the only portion of \mathcal{W}_r that is entangled with the control register.

A. $N = 21 = 3 \times 7$, $a = 2$, $r = 6$

As an example of the method, consider the number $N = 21$ with the base $a = 2$. The work register must contain $n = \lceil \log_2 21 \rceil = 5$ qubits, and therefore takes the form $|w\rangle = |w_4 \cdots w_0\rangle$, where $w = w_4 w_3 w_2 w_1 w_0 \in \{0, 1, \dots, 31\}$ is a 5-bit indexing integer. Note that the ME function $f(x) = 2^x \pmod{21}$ has a period of $r = 6$, as illustrated in Fig. 4. Also note that the state transitions are given by $|1\rangle \rightarrow |2\rangle \rightarrow |4\rangle \rightarrow |8\rangle \rightarrow |16\rangle \rightarrow |11\rangle \rightarrow |1\rangle$. Figure 5 shows the corresponding ME operator $U_{2,21}$, which is partitioned into six levels delimited by the barriers in the circuit. The first partition in the Figure gives $U|1\rangle = |2\rangle$, as the first SWAP gate changes the initial state $|1\rangle = |00001\rangle$ into the next state $|2\rangle = |00010\rangle$. The remaining sequence of gates have no effect on the state $|2\rangle$. In the second partition, the next SWAP operation transforms $|2\rangle = |00010\rangle$ into $|4\rangle = |00100\rangle$, and so on. More precisely, because the gates in each level act successively, the second transition $|2\rangle \rightarrow |4\rangle$ is actually accomplished by the first two partitions: the SWAP gate in $x = 0$ is followed by the SWAP gate in $x = 1$, which performs the operation $|2\rangle \rightarrow |1\rangle \rightarrow |4\rangle$. The remaining partitions have no effect on state $|4\rangle$. Finally, the last partition returns the state $|11\rangle$ back into the



$U w\rangle = 2 \times w \pmod{21}\rangle$	
$U 1\rangle = 2\rangle$	$U 00001\rangle = 00010\rangle$
$U 2\rangle = 4\rangle$	$U 00010\rangle = 00100\rangle$
$U 4\rangle = 8\rangle$	$U 00100\rangle = 01000\rangle$
$U 8\rangle = 16\rangle$	$U 01000\rangle = 10000\rangle$
$U 16\rangle = 11\rangle$	$U 10000\rangle = 01011\rangle$
$U 11\rangle = 1\rangle$	$U 01011\rangle = 00001\rangle$

FIG. 4. $N = 21$, $a = 2$, $r = 6$: The left panel illustrates the modular exponential function $f_{2,21}(x) = 2^x \pmod{21}$, while the right panel shows the action of the modular exponentiation operator $U_{2,21}$ on the closed sequence $[1, 2, 4, 8, 16, 11, 1]$. The circuit requires $n = \lceil \log_2 21 \rceil = 5$ qubits in the work register.

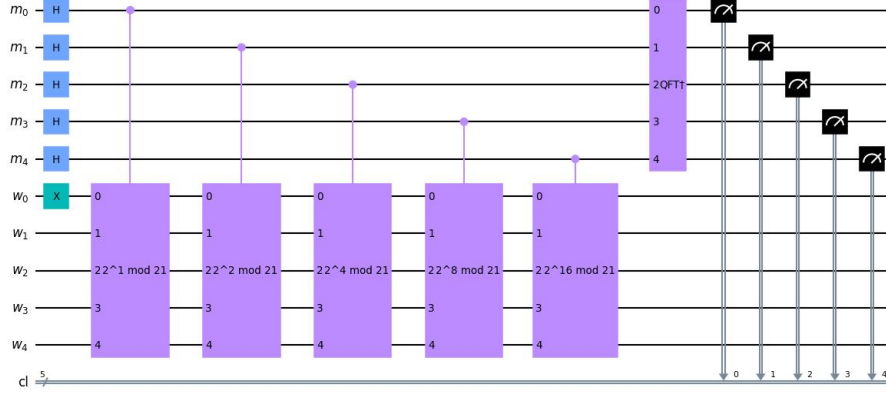


FIG. 6. The Shor factoring circuit in Qiskit for $N = 21$, $a = 2$, $n = 5$, and $m = 5$.

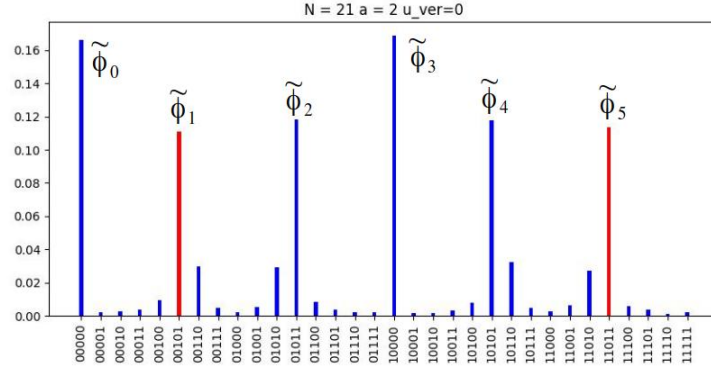


FIG. 7. The phase histogram for $N = 21$, $a = 2$, $n = 5$, and $m = 5$ from a Qiskit simulation with 4096 runs for the concatenated version `u_ver=0`. The abscissa indexes the possible phases, and the ordinate provides their corresponding probabilities. The six dominant peaks of the histogram occur very close to the six eigenphases $\phi_s = s/6$ of the ME operator $U_{2,21}$ for $s \in \{0, 1, \dots, 5\}$. The phases shown in red corresponding to $s = 1$ and $s = 5$ are those that produce the factors of 3 and 7, and they occur at the (binary) values $\tilde{\phi}_1 = 0.00101 \approx \phi_1 = 1/6$ and $\tilde{\phi}_5 = 0.11011 \approx \phi_5 = 5/6$.

corresponds to the 5-bit binary phase $\tilde{\phi} = \tilde{\ell}/2^5 = 0.\tilde{\ell}_4 \dots \tilde{\ell}_0$, where $\tilde{\ell}_k \in \{0, 1\}$ is the measured value of the k -th qubit of the control register. The Table shows that the phases that yield factors are $\tilde{\phi}_1 = 0.00101 \approx \phi_1 = 1/6$ and $\tilde{\phi}_5 = 0.11011 \approx \phi_5 = 5/6$, and the continued fractions algorithm therefore returns the period $r = 6$. The decimal representation of the phase is also provided for convenience, as well as the fractional representation `phi_phase_frc`. The continued fraction of $\tilde{\phi}$ and its associated convergents are also listed, where fractions s/r are denoted by ordered pairs (s, r) . The analysis script loops over the hand full of convergents, testing the period r to check that (i) r is even, (ii) $a^{r/2} \neq -1 \pmod{N}$, and (iii) $a^r = 1 \pmod{N}$. If r is a solution, then the factors are determined by $\gcd(a^{r/2} \pm 1, N)$.

We are now ready to address the concatenation issue. For $m = 5$ qubits in the control register, we require the operators U^2, U^4, U^8 and U^{16} . We have been constructing the com-

TABLE I. The output of Shor's algorithm for $N = 21$, $a = 2$, $n = 5$, and $m = 5$ for 4096 shots. Only the two phase values that produced factors are listed.

```

l_measured    : 00101 5 frequency: 466
phi_phase_bin: 0.00101
phi_phase_dec: 0.15625
phi_phase_frc: (5, 32)
cont frc of phi : [0, 6, 2, 2]
convergents of phi: [(0, 1), (1, 6), (2, 13), (5, 32)]
conv: (0, 1) r = 1 : no factors found
conv: (1, 6) r = 6 : factors
factor1: 7
factor2: 3
conv: (2, 13) r = 13 : no factors found
conv: (5, 32) r = 32 : no factors found

l_measured    : 11011 27 frequency: 458
phi_phase_bin: 0.11011
phi_phase_dec: 0.84375
phi_phase_frc: (27, 32)
cont frc of phi : [0, 1, 5, 2, 2]
convergents of phi: [(0, 1), (1, 1), (5, 6), (11, 13), (27, 32)]
conv: (0, 1) r = 1 : no factors found
conv: (1, 1) r = 1 : no factors found
conv: (5, 6) r = 6 : factors
factor1: 7
factor2: 3
conv: (11, 13) r = 13 : no factors found
conv: (27, 32) r = 32 : no factors found

```

posite operators U^p by simply concatenating the U operator the appropriate number of times; however, this is an extreme waste of quantum gates (although it is a good test to ensure that the U operator is in fact correct). We should nonetheless construct the operators U^p in the same manner (and with the same script) that we originally used for U . As before, the operators U^p are required to act only on the 6-dimensional subspace $\mathcal{U}_{r=6}$ of the full Hilbert space $\mathcal{W}_{n=5}$. Note that U^2 acts on every other element of the sequence $[1, 2, 4, 8, 16, 11, 1]$, producing two closed sub-sequences $[1, 4, 16, 1]$ and $[2, 8, 11, 2]$. Consequently, this operator loops over the states $|f(2x)\rangle$ and $|f(2x+1)\rangle$ for $x \in \{0, 1, 2, \dots\}$. Similarly, the operator U^4 chooses every 4-th element of the sequence, and so on. Therefore, the operators U^2 , U^4 , U^8 , U^{16} act on the following closed sub-sequences:

$$\begin{aligned}
U_{2,21} &: [1, 2, 4, 8, 16, 11, 1] \\
U_{2,21}^2 &: [1, 4, 16, 1] + [2, 8, 11, 2] \\
U_{2,21}^4 &: [1, 16, 4, 1] + [2, 11, 8, 2] \\
U_{2,21}^8 &: [1, 4, 16, 1] + [2, 8, 11, 2] \\
U_{2,21}^{16} &: [1, 16, 4, 1] + [2, 11, 8, 2] .
\end{aligned} \tag{3.4}$$

I have restored the $N = 21$ and $a = 2$ subscripts on the ME operator $U = U_{2,21}$ for clarity. Note that $U_{2,21}^2 = U_{2,21}^8$ and $U_{2,21}^4 = U_{2,21}^{16}$ (the second relation follows from squaring the first).

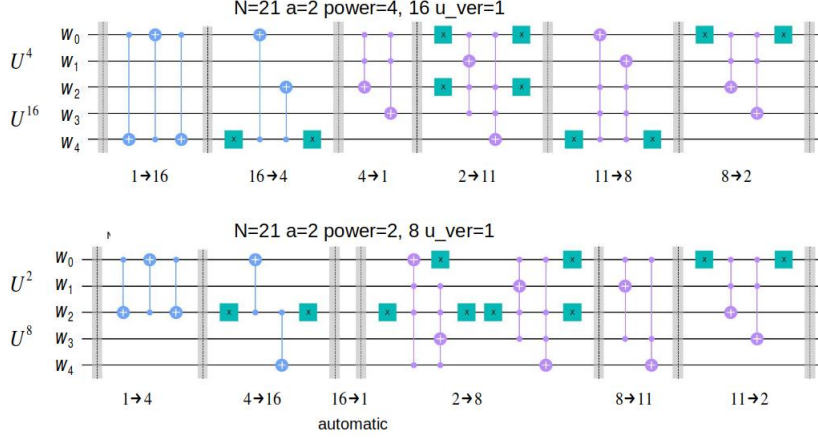


FIG. 8. $N = 21$, $a = 2$, $r = 6$, $n = 5$, $m = 5$: The corresponding composite operators are U^2, U^4, U^8 , and U^{16} . Since $U^2 = U^8$ and $U^4 = U^{16}$, we only need to provide two circuits, which defines version number **u_ver** = 1. The blank barrier in the third level of U^2 and U^8 indicates that the third transition $|16\rangle \rightarrow |1\rangle$ is automatically performed by the first two gates.

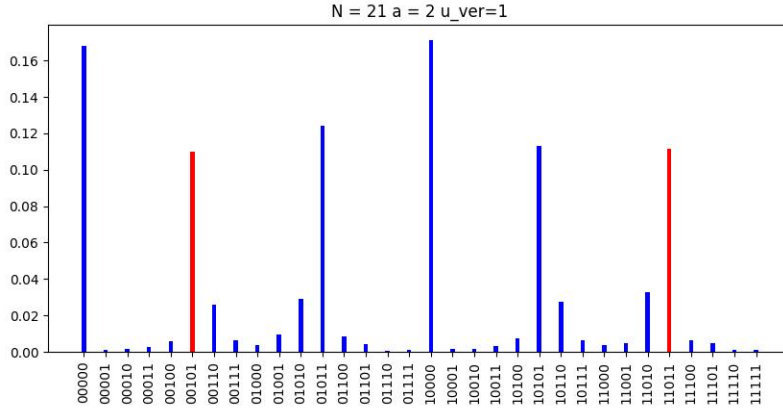


FIG. 9. $N = 21$, $a = 2$, $r = 6$, $n = 5$, $m = 5$: The phase histogram for **u_ver** = 1 agrees exactly with the previous phase histogram of Fig. 7 for **u_ver** = 0, as it should. As before, the phases that produce the factors of 3 and 7 are in red.

The corresponding circuits that produce these sequences are given in Fig. 8, which will be called version number **u_ver** = 1. Note that the third partition is blank for the operators $U_{2,21}^2$ and $U_{2,21}^8$. This means that the first two levels also perform the third transition $|16\rangle \rightarrow |1\rangle$, that is to say, they execute the sequence $|4\rangle \rightarrow |16\rangle \rightarrow |1\rangle$. This occasionally happens when constructing ME operators, and in the future, such blank partitions will signify that they are not required to perform the requisite sequence of transitions (we keep them only to identify the total number of levels in the operator). Finally, Fig. 9 illustrates the phase histogram from the Shor circuit of Fig. 6 using these ME operators. The histogram is identical to that of Fig. 7, as it should be.

At this point, one should levy a serious charge against this procedure: We have used the

entire cycle $[1, 2, 4, 8, 16, 11, 1]$ for the ME operator $U_{2,21}$, which means we know *a priori* that the period of the ME function $f_{2,21}(x)$ is $r = 6$. In other words, if we knew the complete closed sequence for a general number N and base a , then this is equivalent to knowing the period r , and there would be no need for Shor's algorithm. However, it turns out that we do *not* require the complete sequence. This is because the method of continued fractions needs only an *approximate* phase in order to extract the corresponding convergents s/r , and omitting levels in U still provides an adequate approximation for the measured phase $\tilde{\phi}$ (provided we do not omit too many levels). Figure 10 illustrates a *truncated* version of the operators U, U^2, U^4, U^8, U^{16} in which the last 3 levels from each operator have been omitted. The corresponding phase histogram is given in Fig. 11, and shows that employing this truncation strategy still permits us to extract the appropriate phases, and therefore the correct factors. Not surprisingly, the phase histogram has somewhat more noise, but this does not overwhelm the signal.

I shall refer to truncated operators as version `u_ver = 2`, and the truncation level will be specified by the flag `trnc_lv = 0, 1, 2, \dots, r - 1`. The value 0 means that there is no truncation, and all levels are maintained; a value of $k \in \{1, \dots, r - 1\}$ means that the final k segments of the U^p operators have been omitted, leaving only the first $r - k$ levels. For the case $N = 21$ and $a = 2$ with period $r = 6$, there are five nonzero truncation levels, and we have seen that `trnc_lv = 3` still permits factoring (as do truncation levels `trnc_lv = 1, 2`). Figure 12 illustrates the phase histogram for the remaining truncation levels `trnc_lv = 4, 5`.

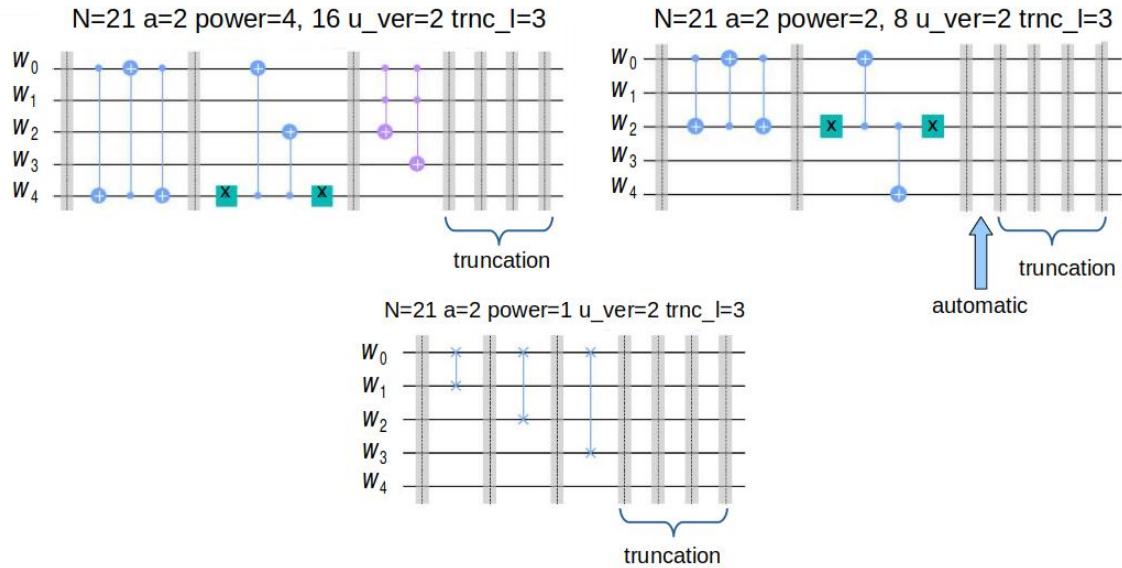


FIG. 10. $N = 21$, $a = 2$, $r = 6$, $n = 5$, $m = 5$: Truncated ME operators U, U^2, U^4, U^8 and U^{16} for version `u_ver = 2` and truncation level `trnc_lv = 3`. This means that the last three levels of the operators have been omitted, which is indicated by the trivial barriers. Note that $U^2 = U^8$ and $U^4 = U^{16}$, and that the first two have an automatic transition at level three.

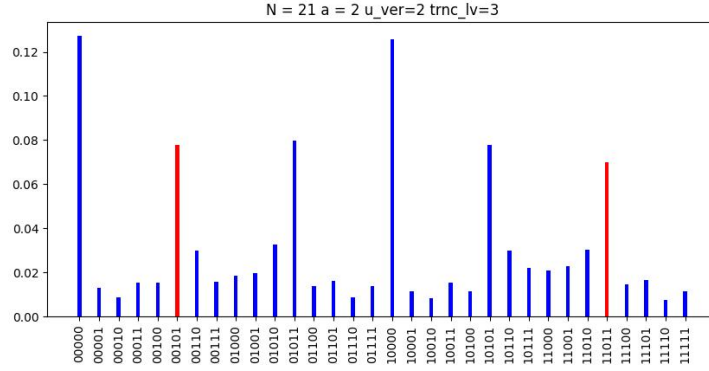


FIG. 11. $N = 21$, $a = 2$, $r = 6$, $n = 5$, $m = 5$: Phase histogram for truncation level `trnc_lv = 3` in which the last three levels have been removed. The signal agrees with the previous two versions, with only slightly more noise, and the peaks in red correspond to phases that produce the factors of 3 and 7.

Even at level 4, in which there are only $6 - 4 = 2$ stages of the ME operators U^p , we are still able to extract factors. It is only for the last truncation level, which retains just a single stage in the ME operators, that the signal recedes into the noise. These results are summarized in Fig. 13 in a quantitative fashion, which plots the average number of tries that are required

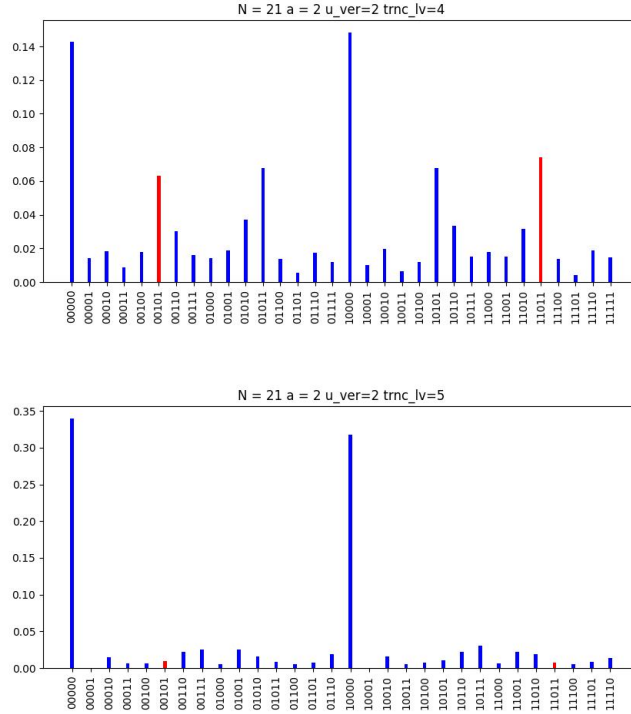


FIG. 12. $N = 21$, $a = 2$, $r = 6$, $n = 5$, $m = 5$: Phase histograms for truncation levels `trnc_lv = 4, 5`. The top panel shows that level 4 truncation, which performs only the first $6 - 4 = 2$ transitions, still permits factorization. In the bottom panel, the signal vanishes at level 5 truncation, where only the first transition is kept.

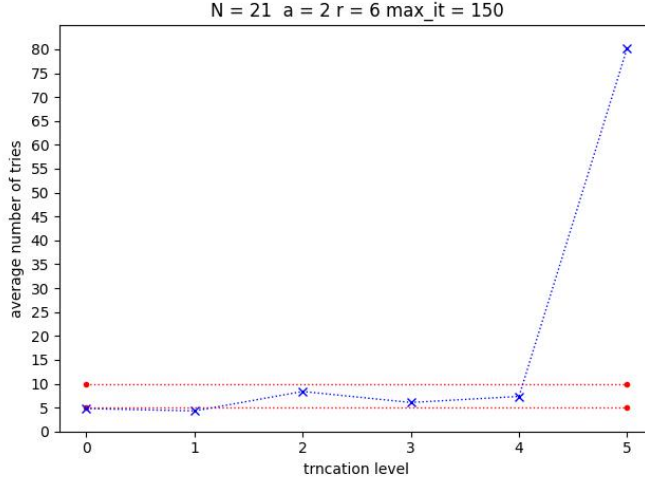


FIG. 13. $N = 21$, $a = 2$, $r = 6$, $n = 5$, $m = 5$: Average number of tries vs. truncation level.

to find a factor as a function of the truncation level. The average was performed with an ensemble of `num_it` = 150 iterations for every truncation level. We can factor $N = 21$ with $a = 2$ for truncation levels `trnc_lv` = 0, 1, \dots , 4 using only 5 to 10 tries. Note the sharp cliff after level 4, in which level 5 requires of order 80 tries. This is actually worse than random, as the phase histogram in bottom panel of Fig. 12 biases the phase toward two major peaks at $\tilde{\phi} = 0.00000$ and $\tilde{\phi} = 0.10000$, neither of which produce factors.

That we can continue to factor when well over half the levels have been omitted is quite remarkable, and if this result continues to hold for larger numbers, it can be exploited for the factorization process. The strategy would be to build the operators U^p one level at a time, checking for factors at each level. For example, in the case of $N = 21$ with $a = 2$, we would start with the first level, finding no factors (`trnc_lv` = 5). We would then proceed to the second level (`trnc_lv` = 4), after which we would find the requisite factors, and there would be no need to continue with higher levels. Apparently, there are enough correlations in the set of truncated operator U^p for $p = 1, 2, 4, 8, 16$ to maintain a sufficiently correlated control register to permit factorization. I will henceforth refer to the concatenated operators by `u_ver` = 0, and the individually constructed composite operators U^p will be denoted by `u_ver` = 1. The truncated operators will be denoted by version number `u_ver` = 2, with the truncation level specified by the flag `trnc_lv` = 0, 1, 2, \dots , $r - 1$.

B. $N = 33 = 3 \times 11$, $a = 7$, $r = 6$

Recall that the difficulty in factoring a specific number N lies not in the size of the number itself, but in the length of the period r of the modular exponentiation function [22]. The ME function for $N = 35$ with base $a = 4$ has a period of $r = 6$, and a systematic truncation-level study reveals that $N = 35$ can be factored with only two levels, just like the previous case for $N = 21$ and $a = 2$. It is more interesting therefore to examine numbers with larger periods. Figure 14 shows that $N = 33$ with base $a = 7$ has a period of $r = 10$. Since the period is larger than the previous case, we require more resolution in the control register, and so we take $m = 6$ qubits. We must therefore construct the operators $U, U^2, U^4, \dots, U^{32}$. As before, the composite operators U^p loop over closed sub-cycles, which in this case become:

$$\begin{aligned}
U_{7,33} &: [1, 7, 16, 13, 25, 10, 4, 28, 31, 19, 1] \\
U_{7,33}^2 &: [1, 16, 25, 4, 31, 1] + [7, 13, 10, 28, 19, 7] \\
U_{7,33}^4 &: [1, 25, 31, 16, 4, 1] + [7, 10, 19, 13, 28, 7] \\
U_{7,33}^8 &: [1, 31, 4, 25, 16, 1] + [7, 19, 28, 10, 13, 7] \\
U_{7,33}^{16} &: [1, 4, 16, 31, 25, 1] + [7, 28, 13, 19, 10, 7] \\
U_{7,33}^{32} &: [1, 16, 25, 4, 31, 1] + [7, 13, 10, 28, 19, 7] .
\end{aligned} \tag{3.5}$$

Note that $U^2 = U^{32}$, and therefore U, U^2, \dots, U^{16} form a complete set of operators (as any other power of p can be obtained by squaring). The composite operators U^p that produce these sequences are illustrated in Fig. 15. Figure 16 shows the results from a

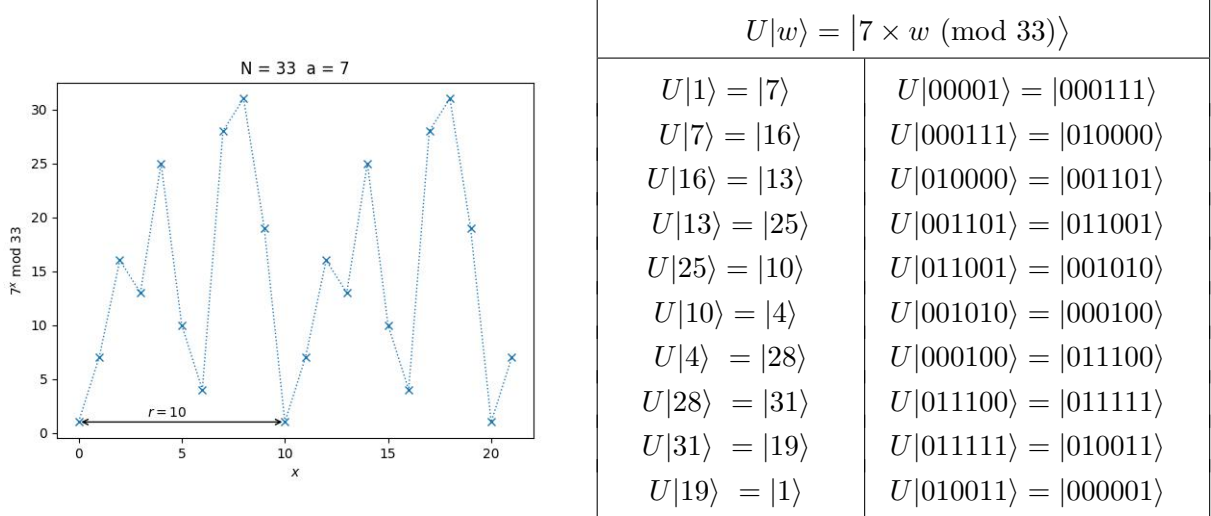


FIG. 14. $N = 33$, $a = 7$, $r = 10$, $n = 6$: The left panel gives the modular exponential function $f_{7,33}(x) = 7^x \pmod{33}$, and the right panel shows the action of the ME operator $U_{7,33}$ on the closed sequence $[1, 7, 16, 13, 25, 10, 4, 28, 31, 19, 1]$. The circuit requires $n = \lceil \log_2 33 \rceil = 6$ qubits in the work register.

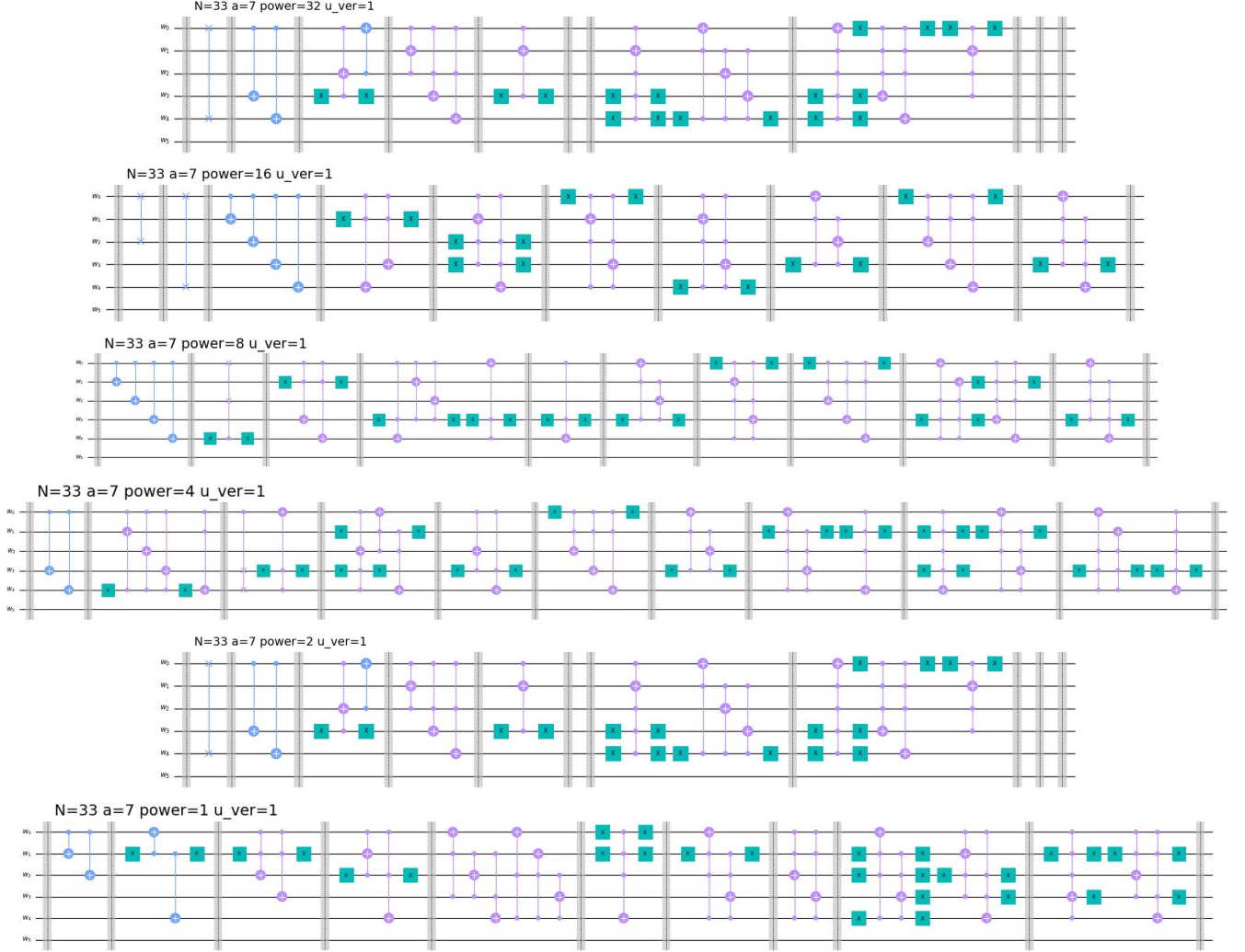


FIG. 15. $N = 33$, $a = 7$, $r = 10$, $n = 6$, $m = 6$: The ME operators U^p for $p = 1, 2, 4, 8, 16, 32$ for version `u_ver` = 1 from bottom to top. Note that $U^2 = U^{32}$.

systematic truncation level study. The top panel gives the phase histogram for `trunc_lv` = 0 (no truncation), and the phase peaks are quite distinct, with little or no noise. The middle panel show the phase histogram for truncation level `trunc_lv` = 6, in which we have kept the first $10 - 6 = 4$ levels. While there is more noise, the signal is still large enough to extract factors with high probability. The lower panel illustrates `trunc_lv` = 7, and we see that the signal has finally receded into the noise. Figure 17 illustrates the average number of tries required to find a factor as a function of the truncation level. For comparison, Fig. 18 illustrates the operators U^p for `trunc_lv` = 6. We see that more than half of the levels can be dropped with enough signal to extract the factors of $N = 33$ with base $a = 7$ and period $r = 10$.

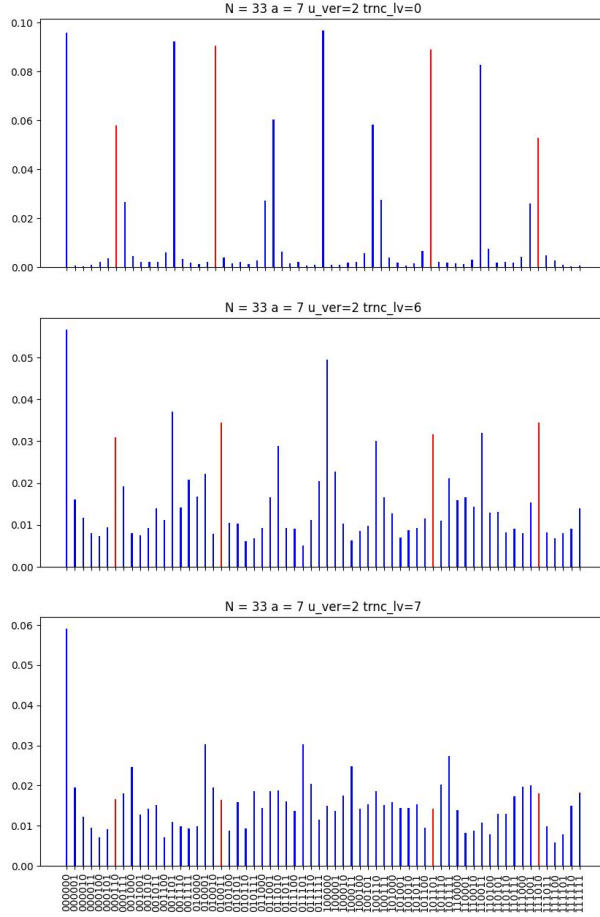


FIG. 16. $N = 33$, $a = 7$, $r = 10$, $n = 6$, $m = 6$: Truncation level study for $\text{trnc_lv} = 0, 6, 7$.

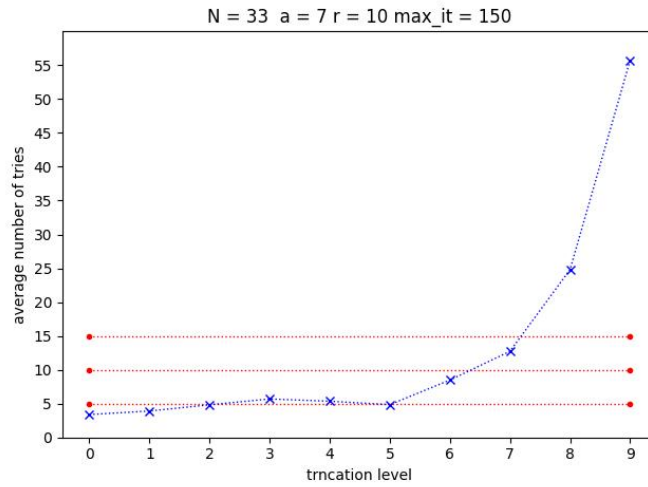


FIG. 17. $N = 33$, $a = 7$, $r = 10$, $n = 6$, $m = 6$: Average number of tries vs. truncation level.

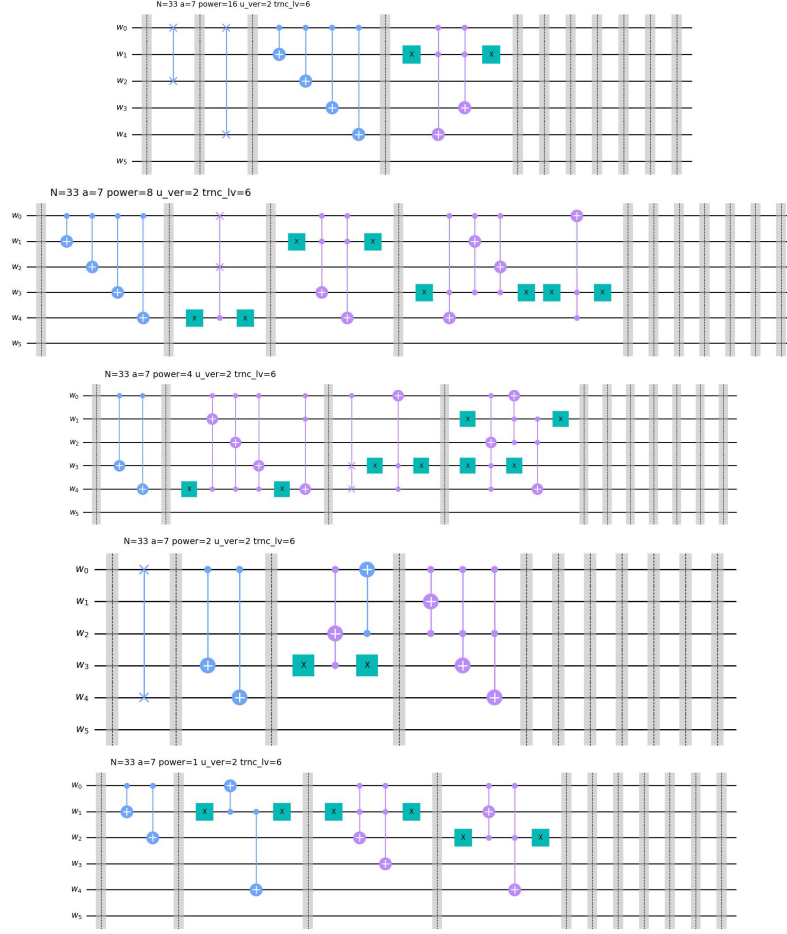
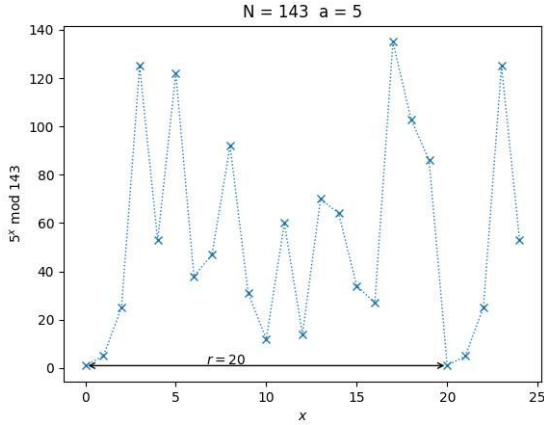


FIG. 18. $N = 33$, $a = 7$, $r = 10$: The truncated ME operators U^p for $p = 1, 2, 4, 8, 16$ for version $u_ver = 2$ and $\text{trnc_lv} = 6$. Since $U^{32} = U^2$, we do not bother to list the $p = 32$ operator.

C. $N = 143 = 11 \times 13$, $a = 5$, $r = 20$

I will now show that this method continues to work for even larger values of N . Let us consider $N = 143$ with $a = 5$, which gives $n = \lceil \log_2 143 \rceil = 8$ work qubits. As illustrated in Fig. 19, the modular exponential function $f_{5,143}(x)$ has a period of $r = 20$, and the corresponding ME operator $U_{5,143}$ is given in Fig. 20. Ideally, we need $m = 2n + 1 = 17$ control qubits; however, since the period is not too large, we can get by with only $m = 8$. We must therefore implement the operators $U_{5,143}, U_{5,143}^2, U_{5,143}^4, U_{5,143}^8, U_{5,143}^{16}, U_{5,143}^{32}, U_{5,143}^{64}$ and $U_{5,143}^{128}$. We will also perform a resolution study on the control register, taking $m = 10$, which requires $U_{5,143}^{256}$ and $U_{5,143}^{512}$.



$U w\rangle = 5 \times w \pmod{143}\rangle$	
$U 1\rangle = 5\rangle$	$U 00000001\rangle = 00000101\rangle$
$U 5\rangle = 25\rangle$	$U 00000101\rangle = 00011001\rangle$
$U 25\rangle = 125\rangle$	$U 00011001\rangle = 01111101\rangle$
$U 125\rangle = 53\rangle$	$U 01111101\rangle = 00110101\rangle$
$U 53\rangle = 122\rangle$	$U 00110101\rangle = 01111010\rangle$
$U 122\rangle = 38\rangle$	$U 01111010\rangle = 00100110\rangle$
$U 38\rangle = 47\rangle$	$U 00100110\rangle = 00101111\rangle$
$U 47\rangle = 92\rangle$	$U 00101111\rangle = 01011100\rangle$
$U 92\rangle = 31\rangle$	$U 01011100\rangle = 00011111\rangle$
$U 31\rangle = 12\rangle$	$U 00011111\rangle = 00001100\rangle$
$U 12\rangle = 60\rangle$	$U 00001100\rangle = 00111100\rangle$
$U 60\rangle = 14\rangle$	$U 00111100\rangle = 00001110\rangle$
$U 14\rangle = 70\rangle$	$U 00001110\rangle = 01000110\rangle$
$U 70\rangle = 64\rangle$	$U 01000110\rangle = 01000000\rangle$
$U 64\rangle = 34\rangle$	$U 01000000\rangle = 00100010\rangle$
$U 34\rangle = 27\rangle$	$U 00100010\rangle = 00011011\rangle$
$U 27\rangle = 135\rangle$	$U 00011011\rangle = 10000111\rangle$
$U 135\rangle = 103\rangle$	$U 10000111\rangle = 01100111\rangle$
$U 103\rangle = 86\rangle$	$U 01100111\rangle = 01010110\rangle$
$U 86\rangle = 1\rangle$	$U 01010110\rangle = 00000001\rangle$

FIG. 19. $N = 143$, $a = 5$, $r = 20$, $n = 8$: The left panel gives the modular exponential function $f_{5,143}(x) = 5^x \pmod{143}$, and the right gives the action of the ME operator $U_{5,143}$ on the closed sequence $[1, 5, 25, 125, 53, 122, 38, 47, 92, 31, 12, 60, 14, 70, 64, 34, 27, 135, 103, 86, 1]$. The Shor circuit requires $n = \lceil \log_2 143 \rceil = 8$ qubits in the work register.

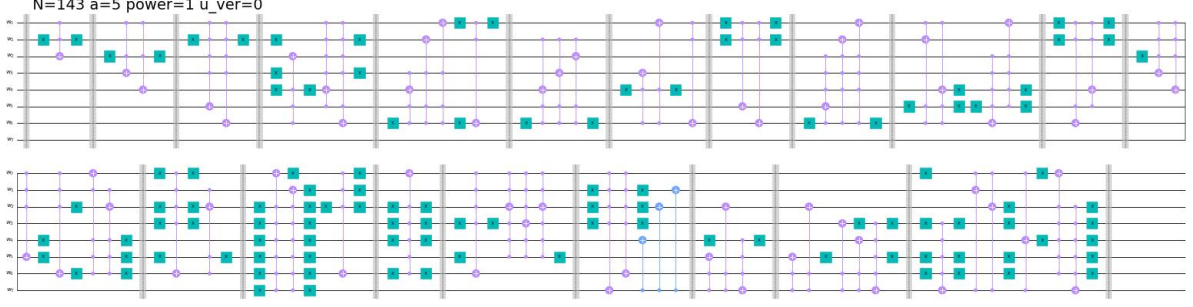


FIG. 20. $N = 143$, $a = 5$, $r = 20$, $n = 8$: The modular exponentiation operator $U_{5,143}$.

The action of the operators $U, U^2, U^4, U^{16}, U^{32}, U^{64}, U^{128}, U^{256}, U^{512}$ are given below:

$$\begin{aligned}
U_{5,143} &: [1, 5, 25, 125, 53, 122, 38, 47, 92, 31, 12, 60, 14, 70, 64, 34, 27, 135, 103, 86, 1] \\
U_{5,143}^2 &: [1, 25, 53, 38, 92, 12, 14, 64, 27, 103, 1] + [5, 125, 122, 47, 31, 60, 70, 34, 135, 86, 5] \\
U_{5,143}^4 &: [1, 53, 92, 14, 27, 1] + [5, 122, 31, 70, 135, 5] + [25, 38, 12, 64, 103, 25] + \\
&\quad [125, 47, 60, 34, 86, 125] \\
U_{5,143}^8 &: [1, 92, 27, 53, 14, 1] + [5, 31, 135, 122, 70, 5] + [25, 12, 103, 38, 64, 25] + \\
&\quad [125, 60, 86, 47, 34, 125] \\
U_{5,143}^{16} &: [1, 27, 14, 92, 53, 1] + [5, 135, 70, 31, 122, 5] + [25, 103, 64, 12, 38, 25] + \\
&\quad [125, 86, 34, 60, 47, 125] \\
U_{5,143}^{32} &: [1, 14, 53, 27, 92, 1] + [5, 70, 122, 135, 31, 5] + [25, 64, 38, 103, 12, 25] + \\
&\quad [125, 34, 47, 86, 60, 125] \\
U_{5,143}^{64} &: [1, 53, 92, 14, 27, 1] + [5, 122, 31, 70, 135, 5] + [25, 38, 12, 64, 103, 25] + \\
&\quad [125, 47, 60, 34, 86, 125] \\
U_{5,143}^{128} &: [1, 92, 27, 53, 14, 1] + [5, 31, 135, 122, 70, 5] + [25, 12, 103, 38, 64, 25] + \\
&\quad [125, 60, 86, 47, 34, 125] \\
U_{5,143}^{256} &: [1, 27, 14, 92, 53, 1] + [5, 135, 70, 31, 122, 5] + [25, 103, 64, 12, 38, 25] \\
&\quad [125, 86, 34, 60, 47, 125] \\
U_{5,143}^{512} &: [1, 14, 53, 27, 92, 1] + [5, 70, 122, 135, 31, 5] + [25, 64, 38, 103, 12, 25] + \\
&\quad [125, 34, 47, 86, 60, 125] ,
\end{aligned} \tag{3.6}$$

where the corresponding circuits are listed in Appendix A 1. Note that $U_{5,143}^4 = U_{5,143}^{64}$, $U_{5,143}^8 = U_{5,143}^{128}$, $U_{5,143}^{16} = U_{5,143}^{256}$, and $U_{5,143}^{32} = U_{5,143}^{512}$ (which can be obtained by squaring the first relation). Figure 21 illustrates the phase histograms for $\mathbf{u_ver} = 1$ for the control resolutions of $m = 8, 10$. The dominant peaks in red correspond to the ME phases $\phi_s = s/20$ with $s \in \{0, 1, \dots, 19\}$ and $\gcd(s, 20) = 1$. Thus the eight phases $s = 1, 3, 7, 9, 11, 13, 17, 19$ provide the factors of 11 and 13. Note, however, that the peaks for $s = 7, 13$ are missing for

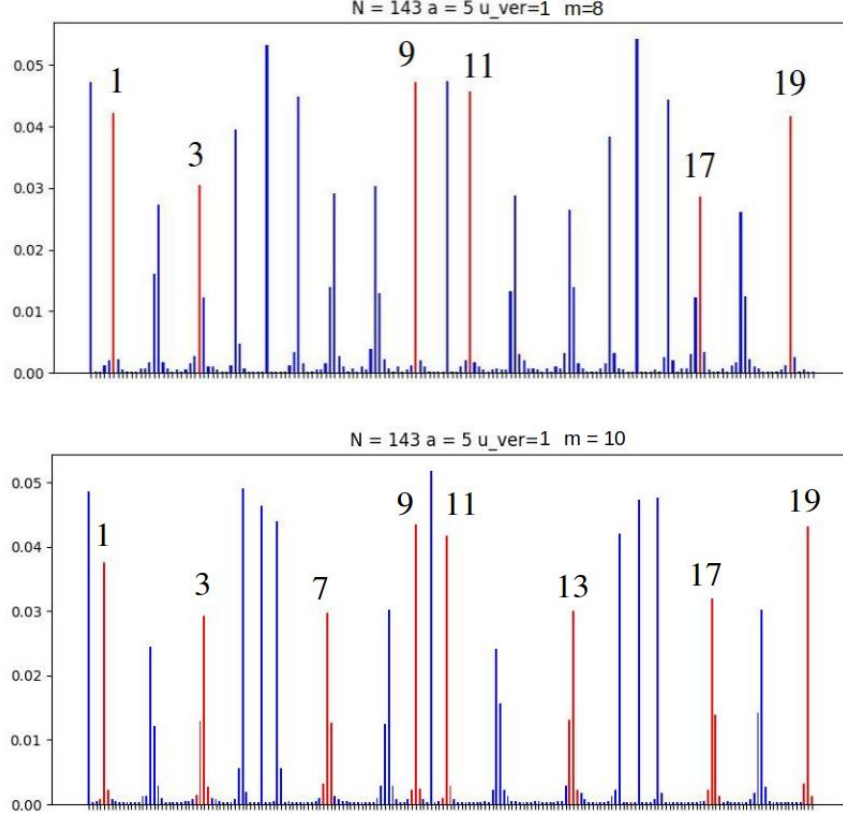


FIG. 21. $N = 143$, $a = 5$, $r = 20$, $n = 8$, $m = 8, 10$: Phase histograms for ME operator version $\text{u_ver} = 1$. The top panel shows $m = 8$, and the bottom panel illustrates the higher resolution $m = 10$. The dominant peaks in red correspond to the ME phases $\phi_s = s/20$ with $s \in \{0, 1, \dots, 19\}$ and $\gcd(s, 20) = 1$. Thus the eight phases $s = 1, 3, 7, 9, 11, 13, 17, 19$ provide the factors of 11 and 13. Note, however, that the peaks for $s = 7, 13$ are missing from the top panel. This is because $m = 8$ does not provide sufficient resolution; however, all peaks are present for $m = 10$.

$m = 8$. This is because $m = 8$ does not provide sufficient resolution, whereas all relevant peaks occur for the choice $m = 10$. Figure 22 shows a truncation study for $m = 8, 10$ over the truncation levels $\text{trnc_lv} = 0, 11, 15, 16, 17$. Since the period is $r = 20$, we can remove more than half the levels before we start to see a degraded signal. To quantify these results, Fig. 23 plots the average number of tries that it takes to obtain a factor *vs.* the truncation level. We see that for $\text{trnc_lv} = 0, 1, \dots, 10$, we can obtain a factor in 5 tries; and for $\text{trnc_lv} = 11, \dots, 15$, we can obtain a factor in under 10 tries. Again, note the steep cliff after level 15. Also note that upon increasing the phase resolution from $m = 8$ to $m = 10$, the signal to noise ratio improves substantially. Increasing the number of control qubits improves the correlations in the work register, and the acceptable truncation level increases slightly for $m = 10$. This trend will turn out to be more pronounced in the next section when we factor the larger number $N = 247$.

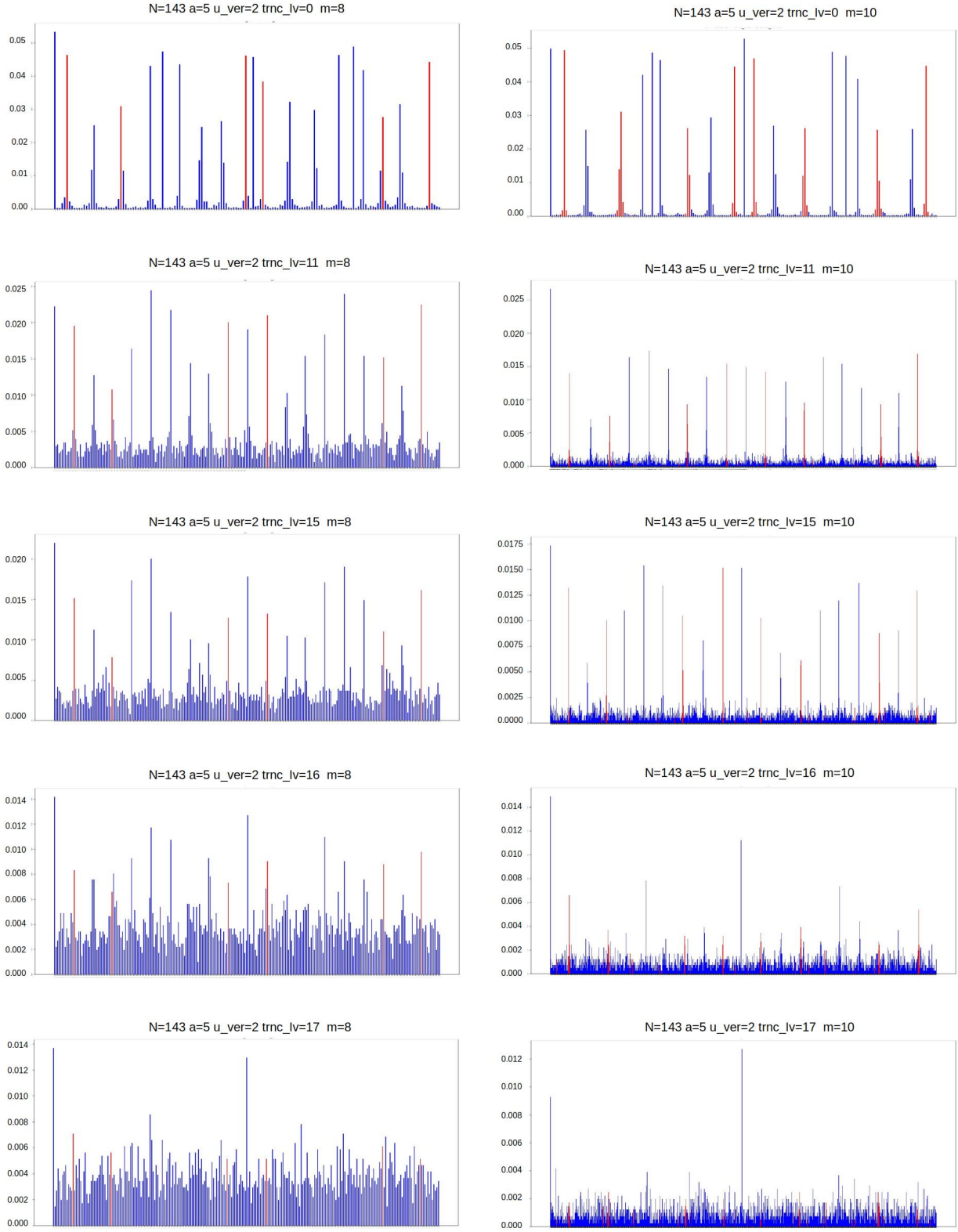


FIG. 22. Truncation study for $N = 143$, $a = 4$, $r = 20$, $n = 8$, $m = 8, 10$. The left panels show $m = 8$, while the right panels are for $m = 10$. The truncation levels are $trnc_lv = 0, 11, 15, 16, 17$. Note that we can extract signals at deeper levels for higher values of m .

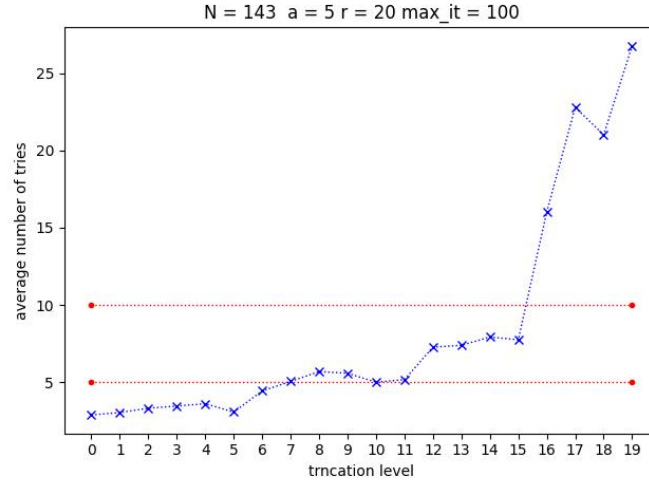
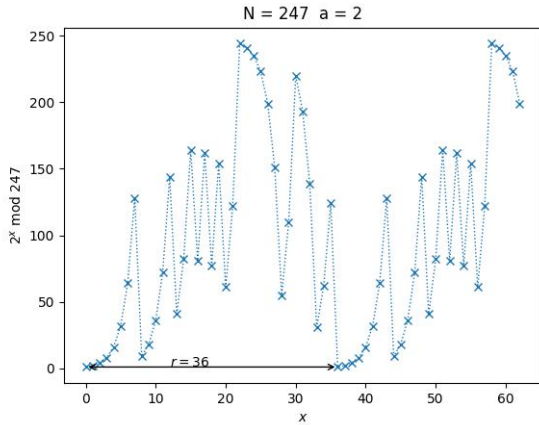


FIG. 23. $N = 143$, $a = 5$, $r = 20$, $n = 8$, $m = 8, 10$: Average number of tries vs. truncation level.

D. $N = 247 = 13 \times 19$, $a = 2$, $r = 36$

We now factor the number $N = 247$ into 13 and 19. For the base $a = 2$, the left panel of Fig. 24 shows that the modular exponential function $f_{2,247}(x)$ has a period of $r = 36$. Note that we require $n = \lceil \log_2 246 \rceil = 8$ work qubits. The action of the ME operator $U_{2,247}$ on the work states $|f_{2,247}(x)\rangle$ is illustrated in right panel of Fig. 24, and its corresponding circuit representation is given in Fig. 25. In the next paragraph, we shall perform a truncation study for $m = 8, 10$ control qubits. We therefore require the ME operators $U_{2,247}^p$ for $p = 1, 2, 4, \dots, 512$. As usual, we construct these operators using the automated gate construction script, as a period of $r = 36$ is so large that manually constructing the composite operators U^p would be too time consuming and error prone.



$U w\rangle = 2 \times w \pmod{247}\rangle$		
$U 1\rangle = 2\rangle$	$U 00000001\rangle = 00000010\rangle$	
$U 2\rangle = 4\rangle$	$U 00000010\rangle = 00000100\rangle$	
$U 4\rangle = 8\rangle$	$U 00000100\rangle = 00001000\rangle$	
$U 8\rangle = 16\rangle$	$U 00001000\rangle = 00010000\rangle$	
$U 16\rangle = 32\rangle$	$U 00010000\rangle = 00100000\rangle$	
$U 32\rangle = 64\rangle$	$U 00100000\rangle = 01000000\rangle$	
$U 64\rangle = 128\rangle$	$U 01000000\rangle = 10000000\rangle$	
$U 128\rangle = 9\rangle$	$U 10000000\rangle = 00001001\rangle$	
$U 9\rangle = 18\rangle$	$U 00001001\rangle = 00010010\rangle$	
$U 18\rangle = 36\rangle$	$U 00010010\rangle = 00100100\rangle$	
$U 36\rangle = 72\rangle$	$U 00100100\rangle = 01001000\rangle$	
$U 72\rangle = 144\rangle$	$U 01001000\rangle = 10010000\rangle$	
$U 144\rangle = 41\rangle$	$U 10010000\rangle = 00101001\rangle$	
$U 41\rangle = 82\rangle$	$U 00101001\rangle = 01010010\rangle$	
$U 82\rangle = 164\rangle$	$U 01010010\rangle = 10100100\rangle$	
$U 164\rangle = 81\rangle$	$U 10100100\rangle = 01010001\rangle$	
$U 81\rangle = 162\rangle$	$U 01010001\rangle = 10100010\rangle$	
$U 162\rangle = 77\rangle$	$U 10100010\rangle = 01001101\rangle$	
$U 77\rangle = 154\rangle$	$U 01001101\rangle = 10011010\rangle$	
$U 154\rangle = 61\rangle$	$U 10011010\rangle = 10011010\rangle$	
$U 61\rangle = 122\rangle$	$U 10011010\rangle = 01111010\rangle$	
$U 122\rangle = 244\rangle$	$U 01111010\rangle = 11110100\rangle$	
$U 244\rangle = 241\rangle$	$U 11110100\rangle = 11110001\rangle$	
$U 241\rangle = 235\rangle$	$U 11110001\rangle = 11101011\rangle$	
$U 235\rangle = 223\rangle$	$U 11101011\rangle = 11011111\rangle$	
$U 223\rangle = 199\rangle$	$U 11011111\rangle = 11000111\rangle$	
$U 199\rangle = 151\rangle$	$U 11000111\rangle = 10010111\rangle$	
$U 151\rangle = 55\rangle$	$U 10010111\rangle = 00110111\rangle$	
$U 55\rangle = 110\rangle$	$U 00110111\rangle = 01101110\rangle$	
$U 110\rangle = 220\rangle$	$U 01101110\rangle = 11011100\rangle$	
$U 220\rangle = 193\rangle$	$U 11011100\rangle = 11000001\rangle$	
$U 193\rangle = 139\rangle$	$U 11000001\rangle = 10001011\rangle$	
$U 139\rangle = 31\rangle$	$U 10001011\rangle = 00011111\rangle$	
$U 31\rangle = 62\rangle$	$U 00011111\rangle = 00111110\rangle$	
$U 62\rangle = 124\rangle$	$U 00111110\rangle = 01111100\rangle$	
$U 124\rangle = 1\rangle$	$U 01111100\rangle = 00000001\rangle$	

FIG. 24. $N = 247$, $a = 2$, $r = 36$, $n = 8$: The left panel is the modular exponential function $f_{2,247}(x) = 2^x \pmod{247}$, while the right panel gives the action of the ME operator $U_{2,247}$. The circuit requires $n = \lceil \log_2 247 \rceil = 8$ qubits in the work register.

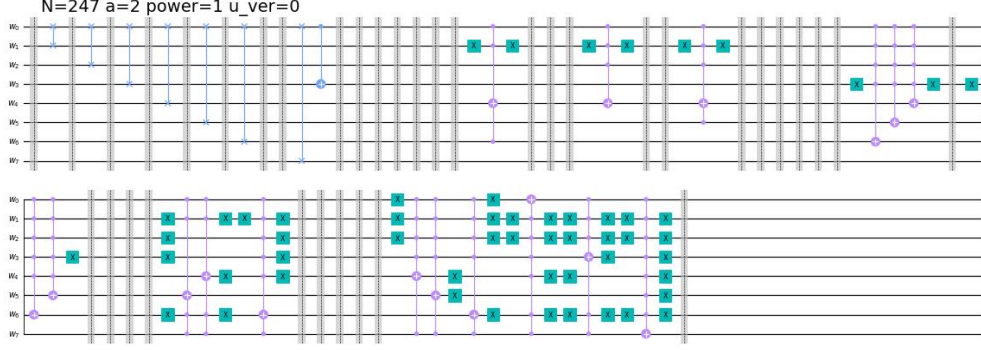


FIG. 25. $N = 247$, $a = 2$, $r = 36$, $n = 8$: The modular exponentiation operator $U_{2,247}$. Note the large number of automatic levels.

The ME operators U^p for $p = 1, 2, 4, \dots, 512$ have the following closed cycles:

$$\begin{aligned}
U_{2,247} &: [1, 2, 4, 8, 16, 32, 64, 128, 9, 18, 36, 72, 144, 41, 82, 164, 81, 162, 77, 154, \\
&\quad 61, 122, 244, 241, 235, 223, 199, 151, 55, 110, 220, 193, 139, 31, 62, 124, 1] \quad (3.7) \\
U_{2,247}^2 &: [1, 4, 16, 64, 9, 36, 144, 82, 81, 77, 61, 244, 235, 199, 55, 220, 139, 62, 1] + \\
&\quad [2, 8, 32, 128, 18, 72, 41, 164, 162, 154, 122, 241, 223, 151, 110, 193, 31, 124, 2] \\
U_{2,247}^4 &: [1, 16, 9, 144, 81, 61, 235, 55, 139, 1] + [2, 32, 18, 41, 162, 122, 223, 110, 31, 2] \\
&\quad [4, 64, 36, 82, 77, 244, 199, 220, 62, 4] + [8, 128, 72, 164, 154, 241, 151, 193, 124, 8] \\
U_{2,247}^8 &: [1, 9, 81, 235, 139, 16, 144, 61, 55, 1] + [2, 18, 162, 223, 31, 32, 41, 122, 110, 2] \\
&\quad [4, 36, 77, 199, 62, 64, 82, 244, 220, 4] + [8, 72, 154, 151, 124, 128, 164, 241, 193, 8] \\
U_{2,247}^{16} &: [1, 81, 139, 144, 55, 9, 235, 16, 61, 1] + [2, 162, 31, 41, 110, 18, 223, 32, 122, 2] \\
&\quad [4, 77, 62, 82, 220, 36, 199, 64, 244, 4] + [8, 154, 124, 164, 193, 72, 151, 128, 241, 8] \\
U_{2,247}^{32} &: [1, 139, 55, 235, 61, 81, 144, 9, 16, 1] + [2, 31, 110, 223, 122, 162, 41, 18, 32, 2] \\
&\quad [8, 124, 193, 151, 241, 154, 164, 72, 128, 8] + [4, 62, 220, 199, 244, 77, 82, 36, 64, 4] \\
U_{2,247}^{64} &: [1, 55, 61, 144, 16, 139, 235, 81, 9, 1] + [2, 110, 122, 41, 32, 31, 223, 162, 18, 2] \\
&\quad [8, 193, 241, 164, 128, 124, 151, 154, 72, 8] + [4, 220, 244, 82, 64, 62, 199, 77, 36, 4] \\
U_{2,247}^{128} &: [1, 61, 16, 235, 9, 55, 144, 139, 81, 1] + [2, 122, 32, 223, 18, 110, 41, 31, 162, 2] \\
&\quad [4, 244, 64, 199, 36, 220, 82, 62, 77, 4] + [8, 241, 128, 151, 72, 193, 164, 124, 154, 8] \\
U_{2,247}^{256} &: [1, 16, 9, 144, 81, 61, 235, 55, 139, 1] + [2, 32, 18, 41, 162, 122, 223, 110, 31, 2] \\
&\quad [4, 64, 36, 82, 77, 244, 199, 220, 62, 4] + [8, 128, 72, 164, 154, 241, 151, 193, 124, 8] \\
U_{2,247}^{512} &: [1, 9, 81, 235, 139, 16, 144, 61, 55, 1] + [2, 18, 162, 223, 31, 32, 41, 122, 110, 2] \\
&\quad [4, 36, 77, 199, 62, 64, 82, 244, 220, 4] + [8, 72, 154, 151, 124, 128, 164, 241, 193, 8] .
\end{aligned}$$

The corresponding circuits are listed in Appendix A 2. Note that $U_{2,247}^4 = U_{2,247}^{256}$ and $U_{2,247}^8 = U_{2,247}^{512}$ (the second relation is given by squaring the first). The phases of the $U_{2,247}$ operator that provide factors occur at $\phi_s = s/36$ for $s \in \{0, 1, \dots, 35\}$, where $r = 36$ and s have no

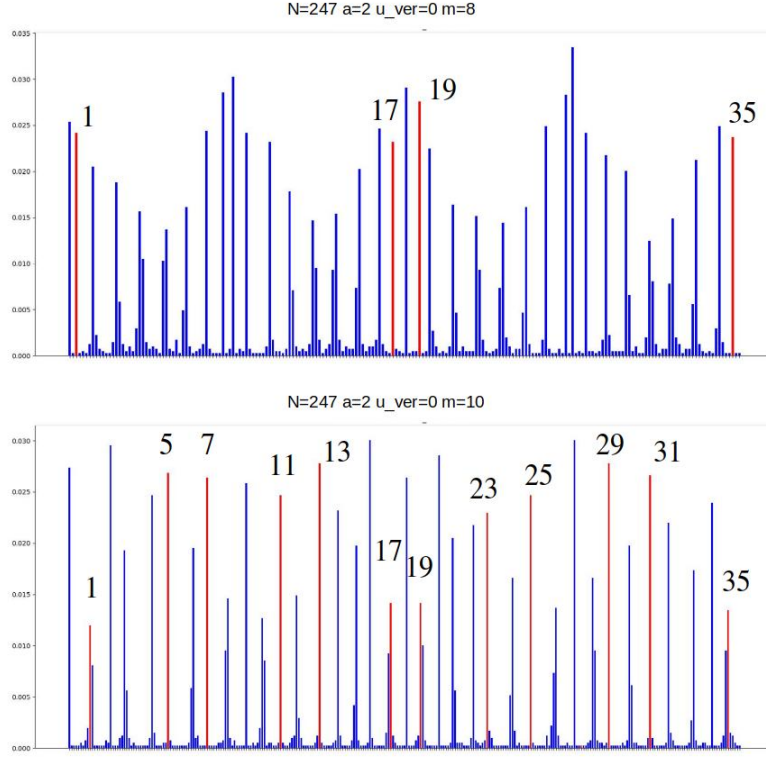


FIG. 26. $N = 247$, $a = 2$, $r = 36$, $n = 8$, $m = 8, 10$: Phase histograms for ME operator version $\mathbf{u_ver} = 1$. The top panel shows $m = 8$, and the bottom panel illustrates the higher resolution $m = 10$. The resolution for $m = 8$ only permits four factorization peaks, while $m = 10$ allows for all twelve.

non-trivial common factors. This gives 12 possible phases: $s = 1, 5, 7, 11, 13, 17, 19, 23, 25, 29, 31, 35$. The phase histograms for $m = 8, 10$ are given in Fig. 26 for $\mathbf{u_ver} = 1$. We see that $m = 8$ only possesses four of these phases, although this is enough to extract factors from Shor's algorithm. However, if we increase the phase resolution to $m = 10$ control qubits, then all 12 phases appear.

Finally, Fig. 27 presents a truncation study for $m = 8, 10$ over the range of truncation levels $\mathbf{trnc_lv} = 0, 10, 20, 25, 30$. The left panels in the Figure show the $m = 8$ results, while the right panels illustrate the corresponding phase histograms for $m = 10$. Note that $m = 8$ starts becoming noisy between $\mathbf{trnc_lv} = 10$ to 20 , but that $m = 10$ retains a strong signal as low as $\mathbf{trnc_lv} = 25$. This means that we only need to keep $36 - 25 = 11$ levels to extract a factorization signal. Finally, Fig. 28 plots the average number of tries required to find a factor *vs.* the truncation level. This is a much more dramatic improvement than in the previous case of $N = 143$, and it will be interesting to see if this trend continues for even larger numbers. However, these studies push the limit of the simulator. Therefore, qubit reduction strategies like qubit recycling [23] must be employed to increase the value of N .

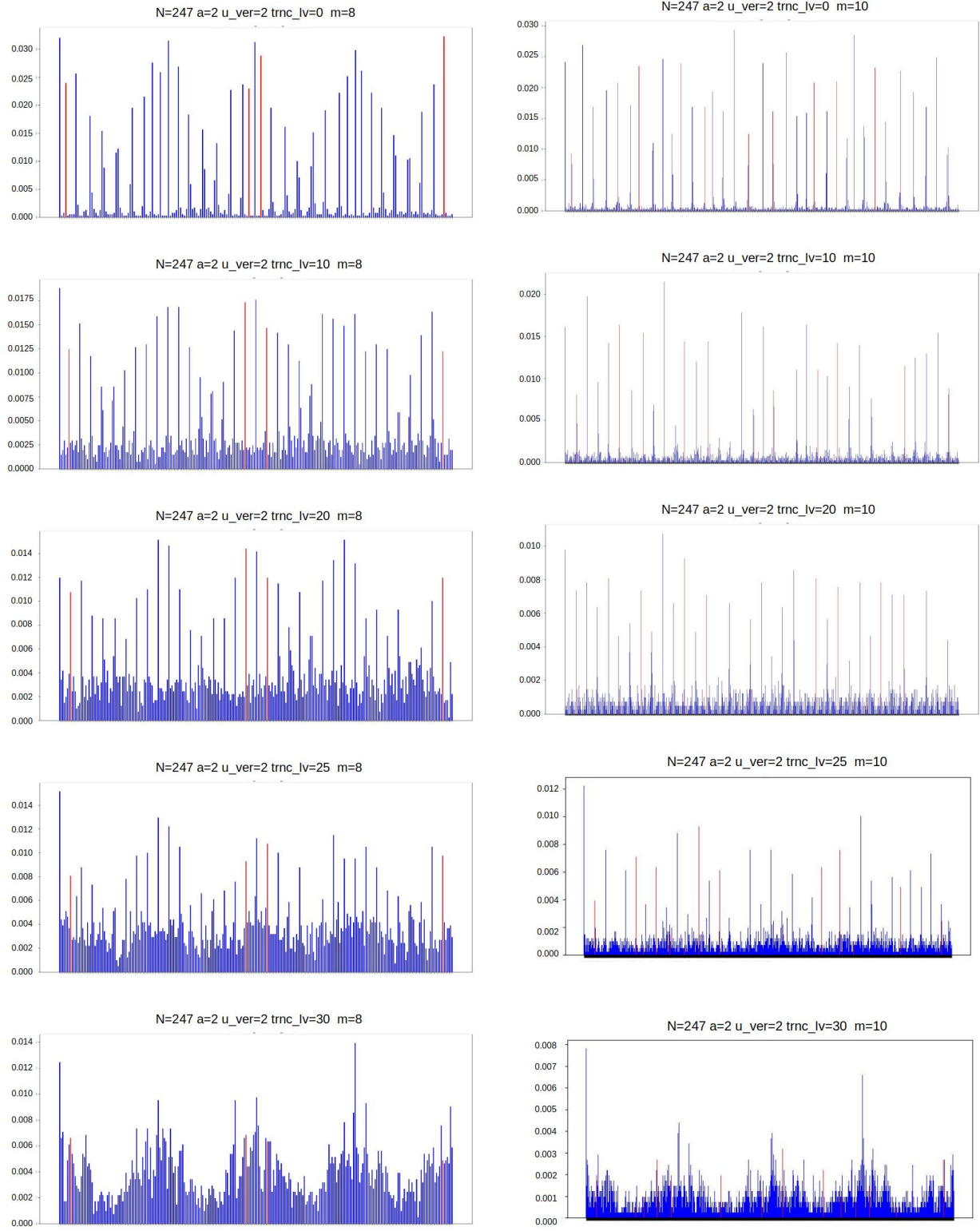


FIG. 27. Truncation study for $N = 247$, $a = 2$, $r = 36$, $n = 8$, $m = 8, 10$ over the range $trnc.lv = 0, 10, 20, 25, 30$, from top to bottom. The left panels show $m = 8$, while the right panels are for $m = 10$. Note that $m = 8$ starts becoming noisy shortly after $trnc.lv = 20$, but that $m = 10$ retains a strong signal as low as $trnc.lv = 25$. In general, the signal is much strong for $m = 10$.

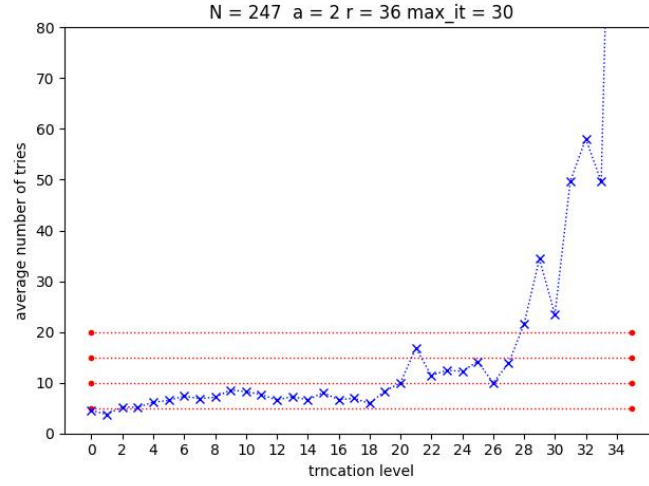


FIG. 28. $N = 247$, $a = 2$, $r = 36$, $n = 8$, $m = 10$: Average number of tries vs. truncation level.

IV. CONCLUSIONS

In this manuscript and in Ref. [16], I have presented a method for constructing modular exponentiation (ME) operators for Shor's algorithm. Because the work register starts in state $|1\rangle$, we do not have to construct a general ME operator acting on the entire 2^n -dimensional Hilbert space \mathcal{W}_n of the work register, as in Ref. [14]. Rather, we only need to construct an operator that acts on the r -dimensional subspace \mathcal{U}_r spanned by the states $|f(x)\rangle$ for $x \in \{0, 1, \dots, r-1\}$. This makes the task far easier, and drastically reduces the qubit count and gate depth as compared to other methods. This approach leads to the following strategy for factoring with Shor's algorithm. Each composite ME operator U^p for $p \in \{2^0, 2^1, \dots, 2^{m-1}\}$ creates closed subsequence of the states in the subspace \mathcal{U}_r . For example, the operator U performs the transition from the state $|f(x)\rangle = |w_n \dots w_1 w_0\rangle$ to the state $|f(x+1)\rangle = |w'_n \dots w'_1 w'_0\rangle$. Transforming a binary number $w = w_n \dots w_1 w_0$ to another binary number $w' = w'_n \dots w'_1 w'_0$, without altering the preceding states, can be turned into a set of formal rules. Therefore, this procedure can be automated using multi-controlled NOT gates and single-qubit NOT gates. Indeed, this is how the ME operators in this manuscript, and in Ref. [16], were constructed. The operator U therefore consists of r levels, where level $x \in \{0, 1, \dots, r-1\}$ performs the transition $U|f(x)\rangle = |f(x+1)\rangle$.

The problem with constructing U in this way is that we must know the period r of the ME function $f(x)$ in advance, and consequently there is no need for Shor's algorithm. However, as I have show in the text, the full sequence of r levels is not required. I perform a number of systematic truncation studies, and find that factorization is still possible even when well over half the levels are omitted. This is because the method of continued fractions, which is used to extract the period r , still provides an adequate approximation to the phase of the U operator. The strategy is then to build the operators U^p one level at a time, checking for factors at each level. The method works because there are enough correlations between the U^p operators to maintain a sufficiently correlated control register that permits factorization.

For intermediate-scale testing, truncation is of clear benefit. However, if the period r becomes exponentially large, this method would seem to require an exponential number of gates. This is likely to happen for an exponentially large number N , which is the case of most interest. We can alleviate this problem by increasing the number of qubits m in the control register, which permits the ME operators to probe deeper. This is because there are more operators U^p for $p \in \{2^0, 2^2, \dots, 2^{m-1}\}$, and therefore more correlations are being tracked. In the coming age of plentiful high quality qubits, increasing m would be of no great concern. I am also investigating other truncation strategies which might alleviate this problem.

Future work will entail factoring larger numbers. Qubit recycling, in which the multi-qubit control register is replaced by a single-qubit register, is an obvious path forward. I am also looking at methods to generalize the construction of the ME operators U^p . By employing templates for the ME operators, we can perhaps find the optimal approximate operator U_{approx}^p for any given U^p . One approach would be to employ a variational quantum method to this end. Finally, it would be interesting to perform a noise study on a simulator to better gauge the effects of real quantum gates on this factoring strategy. This methodology, or generalizations thereof, could help bring Shor's algorithm within closer reach. It remains to be seen just how few levels one can use.

ACKNOWLEDGMENTS

I would like to thank Don Shirk and David Ostby for reading the manuscript for clarity, and for a number of useful discussions.

Appendix A: Modular Exponentiation Operators

1. Modular Exponentiation Operators for $N = 143$

This appendix provides the modular exponentiation (ME) operators $U_{5,143}^p$ for the powers $p \in \{1, 2, 4, \dots, 512\}$. Quantum circuits are often called *scores* because of their resemblance to written musical scores. The quantum score can still be read even when the gates are not quite resolvable to the eye. The green boxes are single-qubit NOT gates X , the blue lines ending with a plus sign in a circle indicate controlled-NOT gates CX , and purple lines with a dots and a circle-plus are multi-controlled-NOT gates $CC \dots CX$.

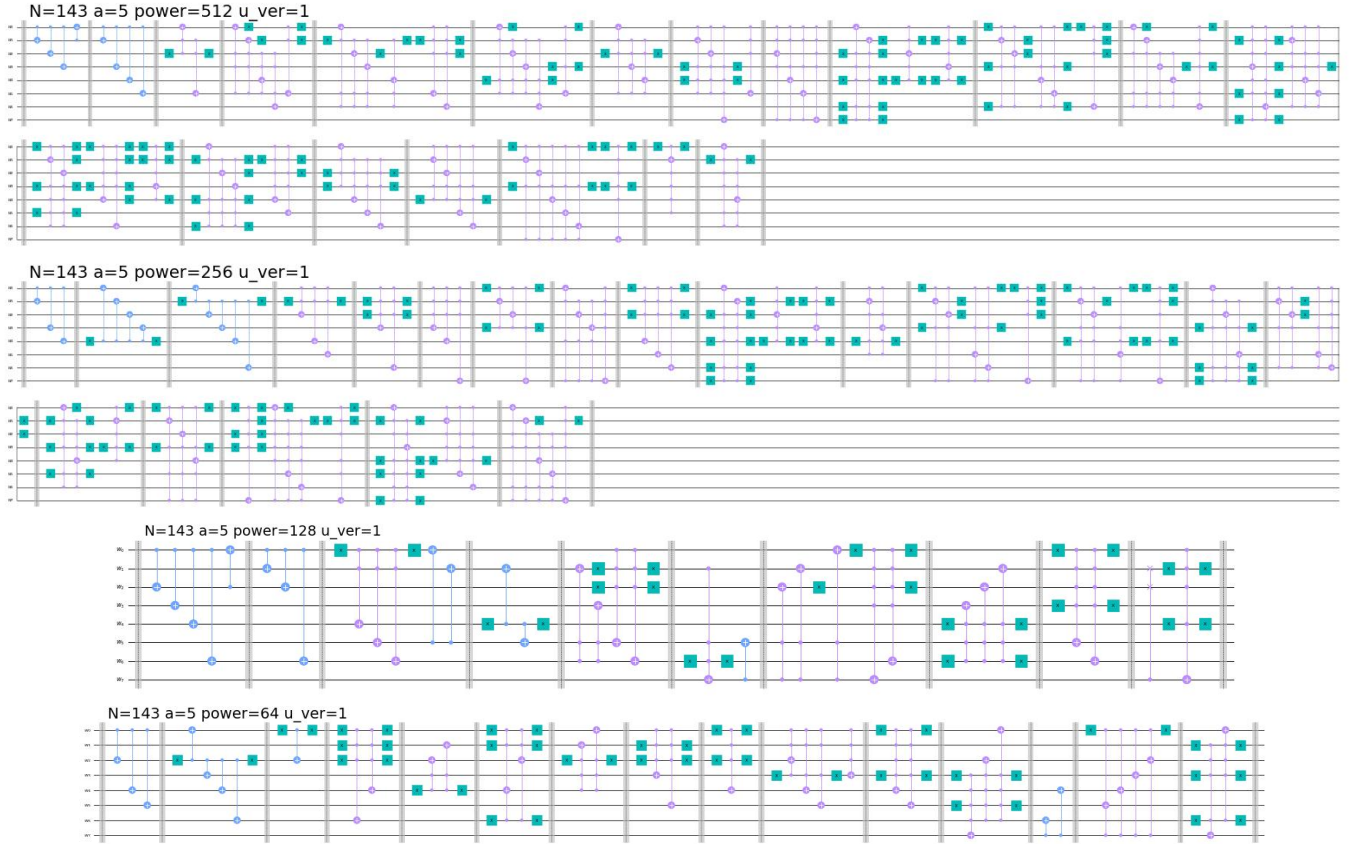


FIG. 29. $N = 143$, $a = 5$, $r = 10$, $n = 8$: The ME operator U^p for the powers $p \in \{64, 128, 256, 512\}$.

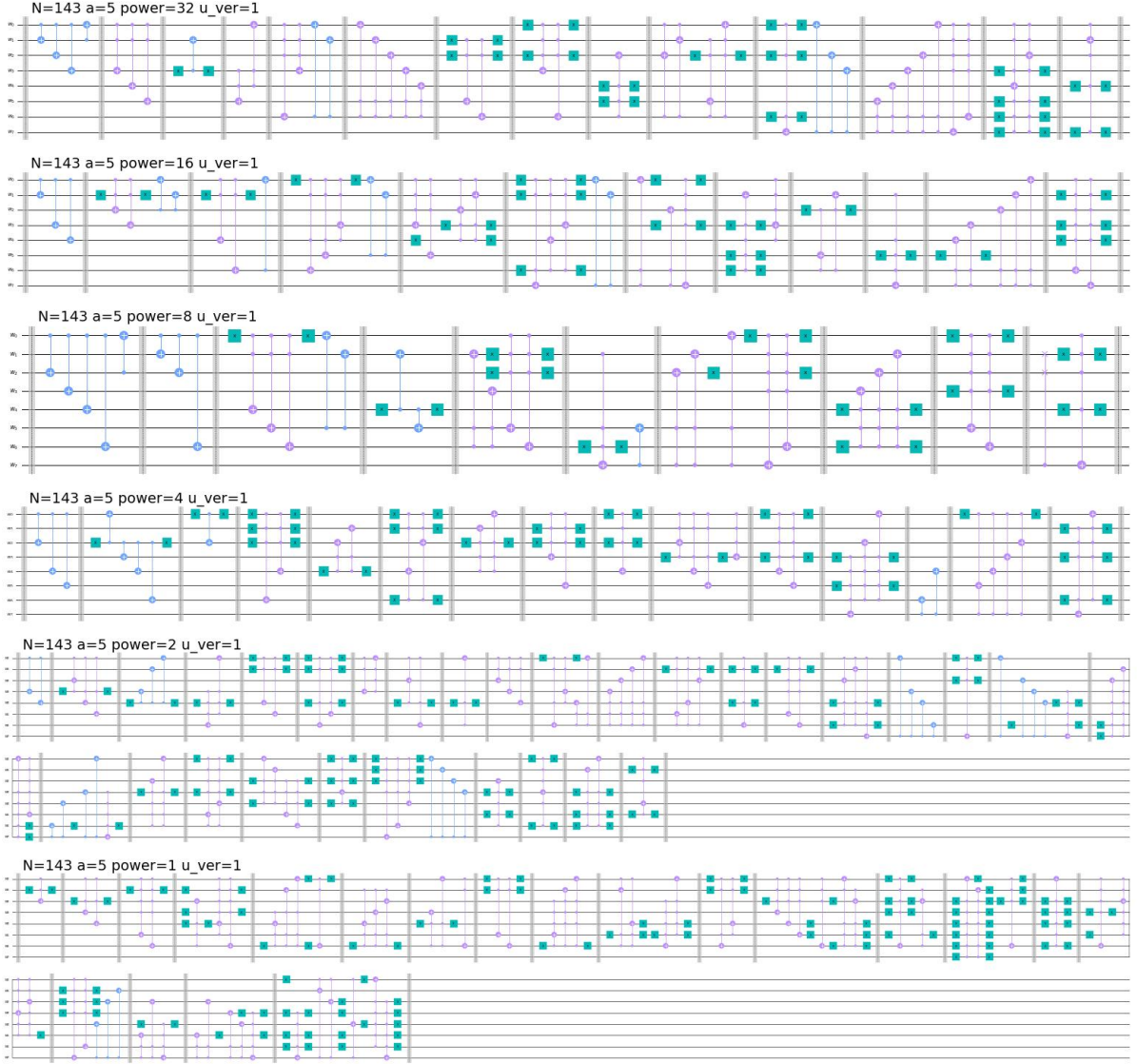


FIG. 30. $N = 143$, $a = 5$, $r = 10$, $n = 8$: The ME operator U^p for the powers $p \in \{1, 2, 4, 8, 16, 32\}$.

2. Modular Exponentiation Operators for $N = 247$

This appendix provides the modular exponentiation (ME) operators $U_{2,247}^p$ for the powers $p \in \{1, 2, 4, \dots, 512\}$. Quantum circuits are often called *scores* because of their resemblance to music. As emphasized in the previous appendix, it is not necessary to resolve every “note” in the *score* of the circuit, as the score can still be read. The green boxes are single-qubit NOT gates X , the blue lines ending with a plus sign in a circle indicate controlled-NOT gates CX , and purple lines with dots and a circle-plus are multi-controlled-NOT gates $CC \dots CX$.

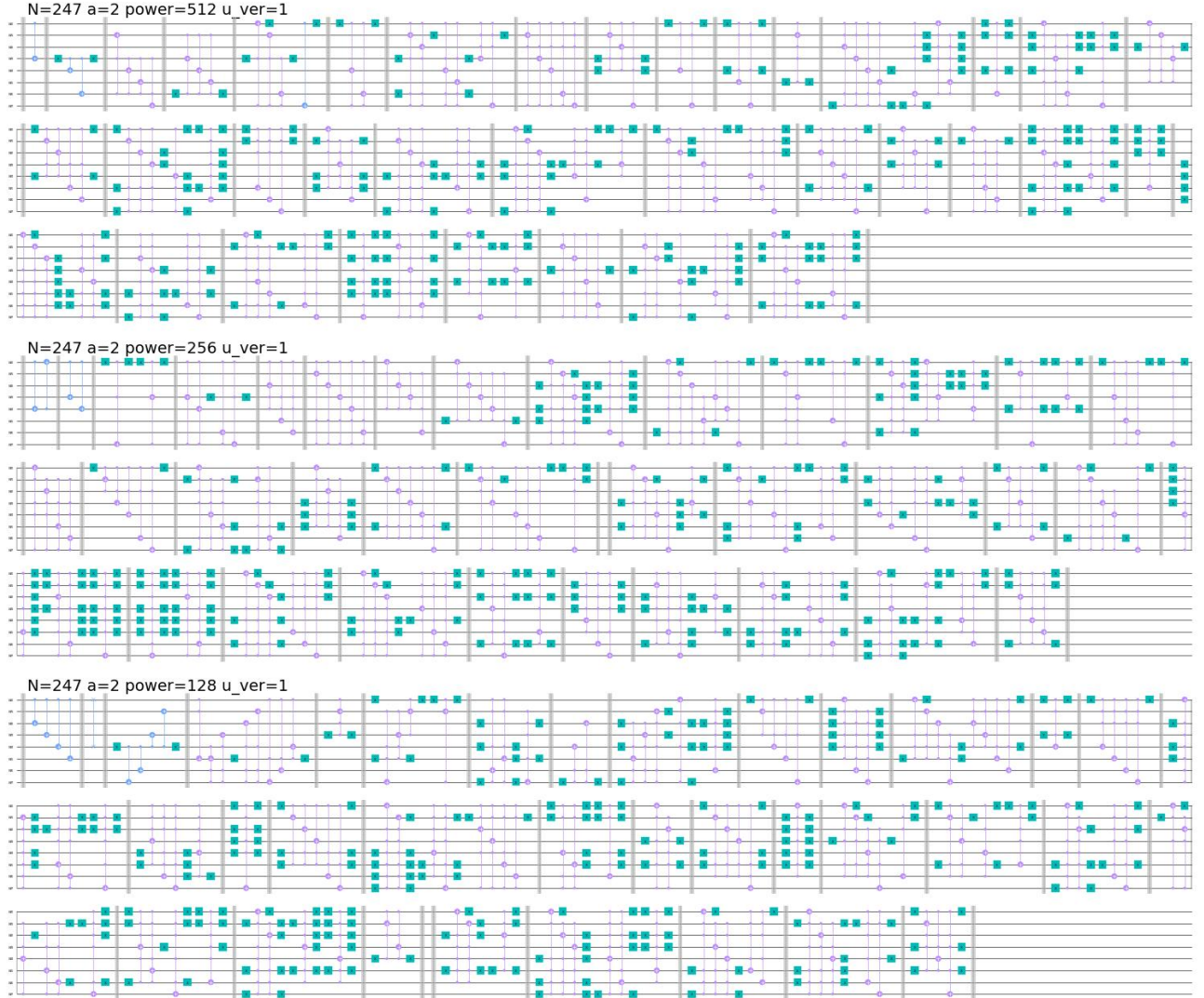


FIG. 31. $N = 247$, $a = 2$, $r = 36$, $n = 8$: The ME operator U^p for the powers $p \in \{128, 256, 512\}$.



FIG. 32. $N = 247$, $a = 2$, $r = 36$, $n = 8$: The ME operator U^p for the powers $p \in \{8, 16, 32, 46\}$.

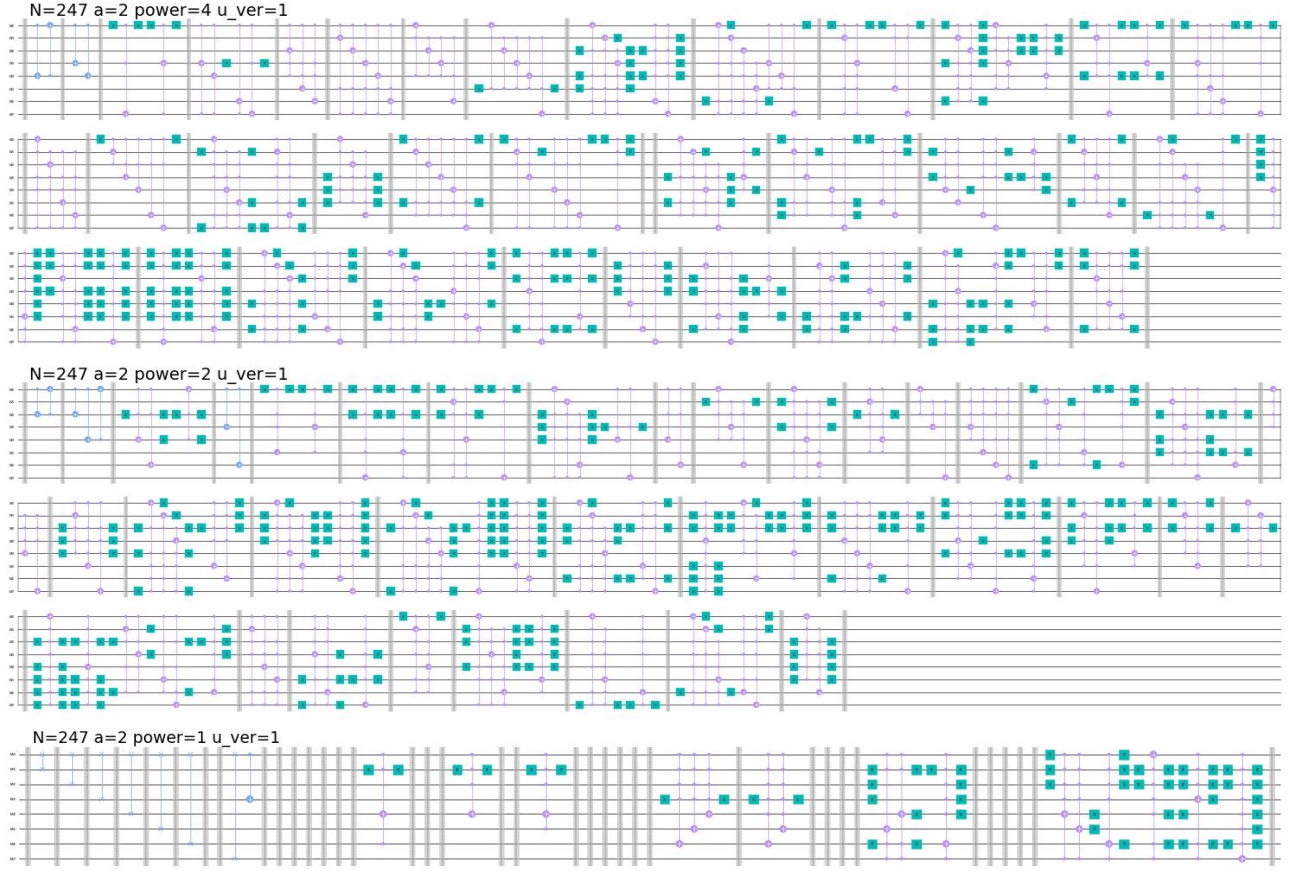


FIG. 33. $N = 247$, $a = 2$, $r = 36$, $n = 8$: The ME operator U^p for the powers $p \in \{1, 2, 4\}$.

-
-
- [1] Ron L Rivest, Adi Shamir, and Leonard Adleman, *A method for obtaining digital signatures and public-key cryptosystems*, Communications of the ACM, **21**(2), 120–126 (1978).
 - [2] Whitfield Diffie and Martin Hellman, *New directions in cryptography*, IEEE Transactions on Information Theory **22** 644–654 (1976).
 - [3] Ralph C Merkle, *Secure communications over insecure channels*, Communications of the ACM **21**(4) 294–299 (1978).
 - [4] P.W. Shor, 35th Annu. Symp. on the Foundations of Computer Science, 124-134 (IEEE Computer Society Press, Los Alamitos, California, 1994).
 - [5] P.W. Shor, *Polynomial-time algorithms for prime factorization and discrete logarithms on a quantum computer*, SIAM J. Comput **26** 1484 (1997).
 - [6] Lieven M. K. Vandersypen, Matthias Steffen, Gregory Breyta, Costantino S. Yannoni, Mark H. Sherwood, Isaac L. Chuang, *Experimental realization of Shor’s quantum factoring algorithm using nuclear magnetic resonance*, Nature 414, 883-887 (20/27 Dec 2001).
 - [7] B. P. Lanyon, T. J. Weinhold, N. K. Langford, M. Barbieri, D. F. V. James, A. Gilchrist, A. G. White, *Experimental demonstration of Shor’s algorithm with quantum entanglement*, Phy. Rev. Lett. **99** 250505 (2007)
 - [8] Chao-Yang Lu, Daniel E. Browne, Tao Yang, Jian-Wei Pan, *Demonstration of Shor’s quantum factoring algorithm using photonic qubits*, Phys. Rev. Lett. **99** 250504 (2007).
 - [9] Alberto Politi, Jonathan C. F. Matthews and Jeremy L. O’Brien, *Shor’s quantum factoring algorithm on a photonic chip*, Science **325** 1221 (2009).
 - [10] Enrique Martin-Lopez, Anthony Laing, Thomas Lawson, Roberto Alvarez, Xiao-Qi Zhou, Jeremy L. O’Brien, *Experimental Realizations of Shor’s quantum factoring algorithm using qubit recycling*, Nature Photonics **6** 773-776 (2012).
 - [11] T Monz, D Nigg, E A Martines, M F Brandl, P Schindler, R Rines, S X Wang, I L Chuang and R Blatt, *Realization of a Scalable Shor Algorithm*, Science **351** (6277) 1068-1070 (2016).
 - [12] Mirko Amico, Zain H. Saleem, Muir Kumph, *An Experimental Study of Shor’s Factoring Algorithm on IBM Q*, Phys. Rev. A **100** 012305 (2019).
 - [13] Unathi Skosana and Mark Tame, *Demonstration of Shor’s factoring algorithm for $N=21$ on IBM quantum processors*, Scientific Reports **11** 16599 (2021).
 - [14] David Beckman, Amalavoyal N Chari, Srikrishna Devabhaktuni, and John Preskill, *Efficient Networks for Quantum Factoring*, Phys. Rev. A **54** 1034-1063 (1996).
 - [15] John Preskill, *Quantum Computing in the NISQ era and beyond*, Quantum **2** 79 (2018) .
 - [16] Robert L Singleton Jr, *Shor’s Factoring Algorithm and Modular Exponentiation Operators*, Quanta **12** 41-130 (2023).
 - [17] Cross, Andrew W., Bishop, Lev S., Smolin, John A., Gambetta, Jay M., *Open Quantum Assembly Language*, arXiv:1707.03429, qiskit-openqasm: OpenQASM specification, International Business Machines, 2017-07-04, retrieved 2017-07-06.
 - [18] Michael A. Nielsen and Isaac L. Chuang, *Quantum Computation and Quantum Information*, Cambridge University Press (2000).

-
- [19] Jiří Tomčala, *On the Various Ways of Quantum Implementation of Modular Exponentiation Function for Shor's Factorization*, International Journal of Theoretical Physics, 63.:14 (2024).
- [20] R Van Meter and K M Itoh, *Fast Quantum Modular Exponentiation*, Phys. Rev. A **71** 052320 (2005).
- [21] Archimedes Pavlidis and Dimitris Gizopoulos, *Fast Quantum Modular Exponentiation Architecture for Shor's Factorization Algorithm*, Quantum Information and Computation **14** 0649-0682 (2014).
- [22] John A. Smolin, Graeme Smith, Alex Vargo, *Oversimplifying quantum factoring*, Nature **499** 163–165 (2013).
- [23] S. Parker and M. B. Plenio, *Efficient factorization with a single pure qubit and $\log N$* , Phys. Rev. Lett. **85** 3049 (2000).